STINFO Copy
AFRL-PR-ED-TR-2006-0041 AFRL-PR-ED-TR-2006-0041

Carbon Materials Research

Wesley P. Hoffman

AFRL/PRSM
9 Antares Road
Edwards AFB CA 93524-7401

August 2006

Final Report

AIR FORCE RESEARCH LABORATORY
AIR FORCE MATERIEL COMMAND
EDWARDS AIR FORCE BASE CA 93524-7048

REPORT DOCUMENTATION PAGE

Form Approved
OMB No. 0704-0188

1. REPORT DATE *(DD-MM-YYYY)*	**2. REPORT TYPE**	**3. DATES COVERED** *(From - To)*
09-08-2006	Final Report	Aug 2004 – Aug 2006

4. TITLE AND SUBTITLE
Carbon Materials Research

5a. CONTRACT NUMBER

5b. GRANT NUMBER

5c. PROGRAM ELEMENT NUMBER
61102F

6. AUTHOR(S)
Wesley P. Hoffman

5d. PROJECT NUMBER

5e. TASK NUMBER
23060529

5f. WORK UNIT NUMBER
549648

7. PERFORMING ORGANIZATION NAME(S) AND ADDRESS(ES)

AFRL/PRSM
9 Antares Road
Edwards AFB CA 93524-7401

8. PERFORMING ORGANIZATION REPORT NO.

9. SPONSORING / MONITORING AGENCY NAME(S) AND ADDRESS(ES)

Air Force Research Laboratory (AFMC)
AFRL/PRSM
9 Antares Road
Edwards AFB CA 93524-7401

10. SPONSOR/MONITOR'S ACRONYM(S)

11. SPONSOR/MONITOR'S REPORT NUMBER(S)
AFRL-PR-ED-TR-2006-0041

12. DISTRIBUTION / AVAILABILITY STATEMENT
Approved for public release; distribution unlimited. Public Affairs AFRL-ERS-PAS-06-217.

13. SUPPLEMENTARY NOTES

14. ABSTRACT

A basic research study in carbon materials for propulsion applications led to research in seemingly diverse areas, which include carbon-carbon composite fabrication, oxidation protection of carbon, microelectromechanical (MEMs) devices, and surface tension phenomena. Carbon-carbon composites are the material of choice in many high temperature thermostructural applications, such as rocket nozzles and exit cones, missile nosetips, and leading edges of hypersonic vehicles. Although these materials are stronger than steel, stiffer than steel, lighter than aluminum, and resistant to thermal shock, they are susceptible to oxidation above 450°C. In addition, they are very costly due principally to the process of densification in which a carbon matrix is placed among the carbon fibers in a perform that has been constructed to have certain mechanical properties. This study has addressed both the problems of oxidation resistance and cost of carbon-carbon composites. In addressing the issue of cost, a completely new and innovative densification approach called *In Situ* densification was conceived and implemented. This process has the dual advantage of both a significant cost reduction as well as a significant reduction in the time needed to densify these composites. In addressing the oxidation protection of carbon-carbon composites, the entirely new field of microtube technology was born. This technology allows the fabrication of free-standing or imbedded microscopic tubes that can possess any cross-sectional or axial shape. Numerous devices have been conceived and fabricated utilizing this technology. Since surface tension is a dominant force at microscopic dimensions, devices employing non-wetting liquids and surface tension were conceived and fabricated. During the fabrication of some of these devices, an entirely new wetting phenomenon was discovered. That is, it is possible to make a non-wetting surface wetting and a wetting surface to be non-wetting simply by changing the geometry of the surface that the liquid contacts.

15. SUBJECT TERMS
carbon-carbon; composites; oxidation; surface tension; oxidation resistance; densification; in situ densification; microtube

16. SECURITY CLASSIFICATION OF:			**17. LIMITATION OF ABSTRACT**	**18. NUMBER OF PAGES**	**19a. NAME OF RESPONSIBLE PERSON**
					Dr. Wesley P. Hoffman
a. REPORT	**b. ABSTRACT**	**c. THIS PAGE**	A	49	**19b. TELEPHONE NO** *(include area code)*
Unclassified	**Unclassified**	**Unclassified**			N/A

Standard Form 298 (Rev. 8-98)
Prescribed by ANSI Std. 239.18

NOTICE AND SIGNATURE PAGE

Using Government drawings, specifications, or other data included in this document for any purpose other than Government procurement does not in any way obligate the U.S. Government. The fact that the Government formulated or supplied the drawings, specifications, or other data does not license the holder or any other person or corporation; or convey any rights or permission to manufacture, use, or sell any patented invention that may relate to them.

This report was cleared for public release by the Air Force Research Laboratory AFRL/PROI Public Affairs Office and is available to the general public, including foreign nationals. Copies may be obtained from the Defense Technical Information Center (DTIC) (http://www.dtic.mil).

AFRL-PR-ED-TR-2006-0041 HAS BEEN REVIEWED AND IS APPROVED FOR PUBLICATION IN ACCORDANCE WITH ASSIGNED DISTRIBUTION STATEMENT.

FOR THE DIRECTOR:

//signature//
WESLEY P. HOFFMAN
Project Manager

//signature//
STEVEN A. SVEJDA
Chief
Propulsion Materials Applications Branch

//signature//
PHILIP A. KESSEL
Technical Advisor
Space and Missile Propulsion Division

This report is published in the interest of scientific and technical information exchange, and its publication does not constitute the Government's approval or disapproval of its ideas or findings.

This Page Intentionally Left Blank

TABLE OF CONTENTS

1.0 EXECUTIVE SUMMARY

1.1 Abstract

A basic research study in carbon materials for propulsion applications led to research in seemingly diverse areas, which include carbon-carbon composite fabrication, oxidation protection of carbon, microelectromechanical (MEMs) devices, and surface tension phenomena.

Carbon-carbon composites are the material of choice in many high temperature thermostructural applications, such as, rocket nozzles and exit cones, missile nosetips, and leading edges of hypersonic vehicles. Although these material are stronger than steel, stiffer than steel, lighter than aluminum, and resistant to thermal shock, they are susceptible to oxidation above 450°C. In addition they are very costly due principally to the process of densification in which a carbon matrix is placed among the carbon fibers in a perform that has been constructed to have certain mechanical properties.

This study has addressed both the problems of oxidation resistance and cost of carbon-carbon composites. In addressing the issue of cost, a completely new and innovative densification approach called In Situ densification was conceived and implemented. This process has the dual advantage of both a significant cost reduction as well as a significant reduction in the time needed to densify these composites.

In addressing the oxidation protection of carbon-carbon composites, the entirely new field of microtube technology was born. This technology allows the fabrication of free-standing or imbedded microscopic tubes that can possess any cross-sectional or axial shape. Numerous devices have been conceived and fabricated utilizing this technology. Since surface tension is a dominant force at microscopic dimensions, devices employing

non-wetting liquids and surface tension were conceived and fabricated. During the fabrication of some of these devices, an entirely new wetting phenomenon was discovered. That is, it is possible to make a non-wetting surface wetting and a wetting surface to be non-wetting simply by changing the geometry of the surface that the liquid contacts.

1.2 Summary and Recommendations

The In Situ densification process produces a very high quality matrix at a fraction of the cost and in a fraction of the time required by current commercial processes. The electrical and thermal conductivity of these composites produced by the In Situ Process exceeds the conductivity of the best commercial composites. In addition, the density of these composites is more uniform than what is available with commercial composites. This is a result of the complete penetration of the liquid matrix precursor into the fiber perform, which is one of the keys of this process. These composites have a wide range of uses in both DOD and commercial applications because of their excellent properties, low cost, and rapid processing time. Application of these composites into full-scale applications, such as exit cones, should be pursued.

Microtubes also have a wide range of application in both DOD and the commercial sector. Applications include cooling, separation technologies, venting and sensors should continue to be pursued.

In normal situations, to change how a liquid interacts with a surface, it is necessary to change either the character of the surface by applying a coating or a surface

treatment or the liquid by, for example, adding a surfactant or solvent. The geometric surface wetting phenomenon allows you to change the wetting character of a surface without changing the character of either the surface or the surface tension of the liquid. This is done simply by physically modifying the surface so that there is an angular surface. This phenomenon has important applications in areas as diverse as heat exchange and catalysis.

2.0 JOURNAL PAPERS

M.B. Dickerson, P.J. Wurm, J.R. Schorr, W.P. Hoffman, P.G. Wapner, and K.H. Sandhage, "Near Net-Shaped, Ultra High Melting, Recession-Resistant Zrc/W-Based Rocket Nozzle Liners Via The Displacive Compensation Of Porosity (DCP) Method," *J. Mat. Sci.*, **39**, 6005-6015 (2004) **(Appendix A).**

W.P. Hoffman, "Material Science of Carbon," Handbook of Materials Modeling, S.Yip, Editor, 2923-2928 (2005) **(Appendix B).**

K. M. Chioujones, W. Ho, P. C. Chau, B. Fathollahi, P. G. Wapner, and W. P. Hoffman, "Microstructural Studies of In-Situ Mesophase Transformation in the Fabrication of Carbon-Carbon Composites," *Carbon*, **44**, 284 (2006) **(Appendix C).**

B. Fathollahi, M. Mauldin, P. C. Chau, P. G. Wapner, and W. P. Hoffman "Integrated Mesophase Injection and In-Situ Transformation in Fabrication of High Density Carbon-Carbon Composites," *Carbon*, 44, 854 (2006) **(Appendix D).**

S.T Iacono, M.W. Perpall, W.P. Hoffman, P.G. Wapner, and D.W. Smith, "Carbonization Studies of Glassy Carbon Derived From Bis-ortho-Diynylarenes (BODA)," *Poly. Prep.,* **47**, 75 (2006) **(Appendix E).**

3.0 PATENTS

"Microtubes with Axially Variable Geometries and Method of Manufacturing Same," Wapner, P.G. and Hoffman W.P., US Pat. No. 6,942,747 (9/13/05)

"Modification of the Degree of Liquid Contact with a Solid by Control of Surface and Micro-Channel Capillary Geometry," Wapner, P.G. and Hoffman W.P., US Pat. No. 6,982,787 (1/3/2006)

This Page Intentionally Left Blank

APPENDIX A

"Near Net-Shaped, Ultra High Melting, Recession-Resistant Zrc/W-Based Rocket Nozzle Liners Via The Displacive Compensation Of Porosity (DCP) Method"

M.B. Dickerson, P.J. Wurm, J.R. Schorr, W.P. Hoffman, P.G. Wapner, and K.H. Sandhage, *J. Mat. Sci.*, **39**, 6005-6015 (2004)

JOURNAL OF MATERIALS SCIENCE **39** (2004) 6005–6015

Near net-shape, ultra-high melting, recession-resistant ZrC/W-based rocket nozzle liners via the displacive compensation of porosity (DCP) method

M. B. DICKERSON
School of Materials Science & Engineering, 771 Ferst Drive, Georgia Institute of Technology, Atlanta, GA 30332, USA

P. J. WURM, J. R. SCHORR
MetaMateria Partners, LLC, 1275 Kinnear Road, Columbus, OH 43212, USA

W. P. HOFFMAN
Air Force Research Laboratory, Edwards Air Force Base, CA 93524, USA

P. G. WAPNER
ERC Inc., Air Force Research Laboratory, Edwards, CA 93523, USA

K. H. SANDHAGE
School of Materials Science & Engineering, 771 Ferst Drive, Georgia Institute of Technology, Atlanta, GA 30332, USA
E-mail: ken.sandhage@mse.gatech.edu

Dense, near net-shaped ZrC/W-based composites have been fabricated at modest temperatures and at ambient pressure by a reactive infiltration process known as the Displacive Compensation of Porosity (DCP) method. Porous WC preforms with hourglass shapes (for rocket nozzle liners) were produced by gel casting, whereas simple bar-shaped preforms were produced by uniaxial pressing. The porous preforms were exposed to molten Zr_2Cu at 1200–1300°C and ambient pressure. The Zr_2Cu liquid rapidly infiltrated into the preforms and underwent a displacement reaction with the WC to yield a more voluminous mixture of solid products, ZrC and W. This displacement reaction-induced increase in internal solid volume filled the prior pore spaces of the preforms ("displacive compensation of porosity") to yield dense, ZrC/W-based composites. Because the preforms remained rigid during reactive infiltration, the final composites retained the external shapes and dimensions of the starting preforms. A DCP-derived, ZrC/W-based nozzle insert was found to be resistant to the severe thermal shock and erosive conditions of a Pi-K rocket motor test. The DCP process enables dense, ceramic/refractory metal composites to be fabricated in complex and near net shapes without the need for high-temperature or high-pressure densification or for extensive machining (i.e., relatively expensive processing steps are avoided).

1. Introduction

The ever more demanding requirements for enhanced performance in aerospace vehicles continue to provide new opportunities for advanced materials. Novel, high-melting, lightweight materials that are chemically, mechanically, and thermally robust are needed to allow for significant improvements in the operating conditions and lifetimes of key rocket and jet engine components [1, 2]. One of the most severe environments encountered in aerospace applications exists in the throat region of a solid-fueled rocket nozzle. Solid, aluminum-bearing fuels generate combustion products (molten aluminum oxide droplets and gas) that impact the nozzles at supersonic speeds and at temperatures in excess of 2500°C [3–5]. Under these extreme conditions, rocket nozzle materials need to exhibit minimal vaporization, erosion, ablation, and creep [1–7]. Nozzle materials must also be highly resistant to thermal shock, given the rapid rise in temperature upon ignition [1, 2, 4, 5, 8]. Among the refractory metallic materials, tungsten possesses the highest melting point (3422°C) and is relatively noble (minimal volatilization and oxidation) under the extreme temperatures and reaction conditions within solid, aluminum-fueled rocket nozzles [9–12]. However, the high density (19.3 g/cm^3), reduction in strength at elevated temperatures, and fabrication costs

0022–2461

for monolithic tungsten make this material less than ideal for rocket components [10–16].

Composites of refractory metals with covalently-bonded ceramics can possess attractive properties for high-temperature rocket applications. Consider, for example, composites of tungsten and zirconium carbide. Zirconium carbide is a hard (up to 2900 kg/mm^2), high melting (up to 3540°C) compound that is considerably lighter than tungsten (the density of ZrC, 6.63 g/cm^3, is about one-third of the density of W) [13, 17, 18]. Tungsten and zirconium carbide are chemically, thermally, and mechanically compatible. These phases exhibit little mutual solid solubility at elevated temperatures (e.g., $\leq$7 mol% at 2800°C) and do not react to form other compounds [19]. Unlike many ceramic/metal composite systems, zirconium carbide and tungsten possess similar thermal expansion coefficients (e.g., 4.5×10^{-6}/°C for W vs. 4.0×10^{-6}/ °C for ZrC at room temperature; 9.2×10^{-6}/ °C for W vs. 10.2×10^{-6}/ °C for ZrC at 2700°C) [20, 21]. Both phases also possess relatively high thermal conductivities (105 ± 10 W/m-K for W, and 40 ± 10 W/m-K for ZrC over the temperature range of 1000–2200°C) [22, 23]. As expected from these thermal properties, ZrC/W composites have been found to be resistant to thermal shock [24]. The carbide phase should endow co-continuous ZrC/W composites with enhanced high-temperature stiffness and creep resistance relative to monolithic tungsten, whereas the ductility of tungsten above 400°C (i.e., above the brittle-to-ductile transformation temperature) should provide enhanced resistance to fracture relative to monolithic zirconium carbide [10, 11, 14–16, 18]. Indeed, Song *et al*. have reported that a W/ZrC composite with 30 vol% ZrC possessed enhanced stiffness relative to monolithic tungsten at 1200°C (about 345 GPa for W/ZrC vs. about 270 GPa for W) [25]. Such composites also exhibited flexural strengths (three-point bending) of 810 MPa at 1200°C [25].

Although dense ZrC/W composites have been produced by high-temperature hot pressing (e.g., at 2000°C and 20 MPa [24–26]), this process is relatively slow and expensive, and is not well-suited for the fabrication of complex-shaped composites such as rocket nozzles. An attractive alternative method for fabricating dense carbide/refractory metal composites in complex shapes is the recently-patented Displacive Compensation of Porosity (DCP) method [27–35]. To date, the DCP process has been used to fabricate a variety of dense, near net-shaped ceramic/metal composites (e.g., MgO/Mg-Al, $MgAl_2O_4$/Fe-Ni-Al, MgO/FeAl, ZrC/W) at modest temperatures [27–35]. However, such prior work involved the fabrication of dense composites with relatively simple shapes (disks, bars, plates). The goal of this paper is to demonstrate that the DCP method can be used to fabricate complex-shaped, ZrC/W-based rocket nozzle inserts. The performance of such nozzles in a solid-fueled rocket test is also discussed in this paper.

2. DCP approach

With the DCP process, a shaped, porous ceramic preform is infiltrated at ambient pressure with a low-melting, reactive metallic liquid. Upon infiltration, the liquid undergoes a displacement reaction with the ceramic preform to generate new ceramic and metal phases within the preform. Unlike other reactive infiltration methods, reactions are chosen that yield a ceramic product with a larger molar volume than the ceramic reactant [27, 28]. Hence, as the displacement reaction proceeds within the infiltrated preform, the prior pore volume becomes filled with new solid ("displacive compensation of porosity"). The excess metallic liquid is then gradually squeezed back out into the surrounding liquid bath, so that a dense, ceramic-rich composite is produced. If the porous preform is lightly sintered prior to infiltration, so that the ceramic particles in the preform are necked, then the preform remains rigid as the internal network of reactant ceramic is replaced by the more voluminous solid product(s). The process is completed when either the ceramic reactant is fully consumed or the pores become filled with solid material, which ever happens first. In the latter case, the kinetics of reaction slow appreciably prior to complete consumption of the reactant ceramic phase. The final dense composite retains the shape and dimensions of the starting rigid preform (i.e., near net-shape processing). By using thermodynamically-favored internal reactions at modest temperatures to generate desired high-temperature phases and to fill porosity, the DCP process avoids the need for densification by high-pressure or high-temperature sintering. Furthermore, low-cost conventional ceramic processes (e.g., slip casting, gel casting, powder injection molding, etc.) may be used to produce porous ceramic preforms with complex shapes that are then preserved upon DCP conversion. That is, extensive, time-consuming, and costly diamond machining of green or sintered ceramic bodies is not required to obtain complex shapes.

In the present work, the following type of liquid/solid displacement reaction was used to convert porous WC preforms into dense ZrC/W-based composites:

$$\frac{1}{2}Zr_2Cu(l) + WC(s) \rightarrow ZrC(s) + W(s) + \frac{1}{2}Cu(l) \quad (1)$$

This reaction is of the DCP type; that is, the sum of the molar volumes of the solid products, ZrC and W, is twice the molar volume of solid WC (i.e., V_m[ZrC] + V_m[W] = $2.01V_m$[WC]) [13]. Reaction (1) is also strongly favored from a thermodynamic perspective. Using available thermodynamic data for ZrC, WC, and Zr-Cu liquids, the Gibbs free energy change per mole of reaction (1) at 1300°C is calculated to be −135.2 kJ [36–38]. A Zr_2Cu melt was used in this reaction, instead of pure liquid zirconium, in order to reduce the temperature required for melting and infiltration processing (i.e., to avoid the energy costs and complications associated with handling pure zirconium liquid, which melts at 1855°C [39]). Although comprised of two-thirds zirconium, Zr_2Cu melts congruently at only 1025°C (note: a congruently-melting Zr-Cu compound was preferred, in order to avoid phase separation and uncontrolled segregation during melt infiltration) [39]. Another important consideration in selecting Cu as an alloying element for the Zr-bearing melt was the minimal chemical

reaction of Cu with ZrC and with W. Copper does not react with zirconium carbide to form a more stable carbide [36, 40]. Stable compounds also do not form between Cu and W at ambient pressures, and the solidus temperature of tungsten is only slightly reduced in the presence of copper (from 3422 to 3414°C) [9]. Indeed, copper has been intentionally introduced as a secondary phase in tungsten-based, solid-fueled rocket nozzles for enhanced transpirational cooling (i.e., the latent heats of fusion and of vaporization of copper can be used to absorb some of the heat experienced by a solid-fueled rocket nozzle) [12, 41].

3. Experimental procedure

Composites of zirconium carbide and tungsten were generated by the reactive infiltration of Zr_2Cu(l) into porous tungsten carbide preforms. WC preforms in the shape of an hourglass (for rocket nozzle inserts) were prepared by gel casting. An aqueous solution containing 6.4 wt% of a proprietary gelling agent (MetaMateria Partners, LLC, Columbus, OH) was first prepared. WC powder (99.9% purity, 5.6 μm ave. size, Novel Technologies, Inc., Morristown, TN) was then added to this solution to obtain a mixture comprised of 43 vol% WC. The mixture was then was cast into an aluminum mold. After allowing the casting to set for 45 min, the mold was removed and the casting was allowed to dry at room temperature and then overnight at 55°C. The casting was then heated in flowing Ar to 400°C for 4 h (to remove the organic material) and then to 1450°C for 4 h (to produce rigid porous preforms). WC preforms in the shapes of bars were also prepared by uniaxial pressing of a mixture of the WC powder with 5 wt% of an aqueous solution of 4 wt% polyvinyl alcohol (Airvol 2005 PVA, Air Products and Chemicals, Allentown, PA). The mixture was uniaxially pressed into bars (11 mm long × 9.9 mm wide × 2.5 mm thick) at a peak stress of 300–340 MPa. The green bars were heated to 400°C for 4 h in flowing Ar (to remove the PVA binder) and then to 1600–1700°C for up to 2 h in a vacuum furnace (to produce rigid porous preforms).

Zr_2Cu ingots were prepared by induction melting or by arc melting. For induction melting, a 1 kg charge comprised of zirconium sponge (99.6% purity, 0.8–19 mm dia. pieces, Johnson-Matthey, Ward Hill, MA) and a copper rod (99.99% purity, 2.5 cm dia. × 5.9 cm thick, Atomergic Chemetals, Farmingdale, NY) were placed within a magnesia crucible (96% dense, 10.2 cm dia. × 15.2 cm high, Ozark Technical Ceramics, Webb City, MO). The charge was then sealed within a silica enclosure located inside a water-cooled copper coil connected to a 60 kV induction power supply (Mark IV, Inductotherm, Rancocas, NJ). After repeated evacuation and backfilling with argon, the charge was induction melted and stirred for 4 min. Inductively-coupled plasma spectroscopy (Optima 3000 ICP-OES, Perkin Elmer Corp., Norwalk, CT) indicated that the solidified ingot possessed a composition of 67.5 at% Zr/32.5 at% Cu, which was close to the desired Zr_2Cu composition (note: for ICP analyses, 100 mg of the solidified ingot was completely dissolved in an aqueous solution containing 8 vol% HF and 22 vol% HCl). X-ray diffraction (XRD) analyses of the ground ingot also revealed peaks consistent with Zr_2Cu. Arc melted Zr_2Cu ingots were prepared by ACI Alloys, Inc. (San Jose, CA). Charges of 0.6 kg comprised of a mixture of zirconium chips (99.8 wt% purity, 1 cm × 1 cm × 0.1 mm thick) and copper cylinders (99.99 wt% purity, 6 mm dia. × 4 cm long) were melted with a single arc on a water-cooled copper hearth into disk-shaped ingots (8–10 cm dia. × 1.3 cm thick). To allow for homogenization, each ingot was flipped and remelted, with a total exposure time to the arc of at least 15 min. XRD analyses of the solidified arc-melted ingots yielded peaks consistent with Zr_2Cu.

Reactive infiltration of the nozzle-shaped WC preforms was conducted by immersion in a Zr_2Cu(l) bath. Prior to immersion, the nozzle-shaped preform was suspended above the bath on a graphite support. The Zr_2Cu(l) bath was contained within a cylindrical magnesia crucible (96% dense, 15.2 cm dia. × 15.2 cm tall, Ozark Technical Ceramics). The molar ratio of Zr_2Cu in the bath to WC in the preform was 8.8:1, which was well in excess of the amount required for complete consumption of the WC. After thermal equilibration of the preform and the bath at 1200°C in a 3% H_2/Ar flowing gas atmosphere, the preform was lowered into the Zr_2Cu(l) bath. After immersion for 10 min, the preform was raised above the bath and heated at 2°C/min to 1300°C. This increase in temperature was conducted to enhance the rate of chemical reaction after the molten metal had infiltrated into the preform. The preform was then cooled to room temperature. For the smaller bar-shaped WC preforms, pieces of the solid Zr_2Cu ingot were placed on top of the WC plates within a flat-bottomed magnesia combustion boat (96% dense, 1.27 cm deep × 10.2 cm long × 5.1 cm wide, Ozark Technical Ceramics). The molar ratio of Zr_2Cu:WC used in the bar infiltration experiments was maintained at 1.5–1.6:1, (i.e., in excess of the amount required for complete consumption of the WC). The Zr_2Cu-covered preforms were heated at 7°C/min to 1200–1300°C for 1–8 h and then cooled at 7°C/min to room temperature. The phase content and microstructure of the resulting composites were evaluated with a scanning electron microscope (XL-30 SEM, Philips Electron Instruments, Eindhoven, The Netherlands) equipped with an energy-dispersive X-ray (EDX) detector (Edax International, Mahwah, NJ) and with XRD analyses. Image analyses (Clemex Vision 3.0.027 image analyses software, Langueuil, Quebec, Canada) of backscattered electron images ($\geq$10 images per sample) were conducted to determine the phase contents of the reacted composites.

A composite rocket nozzle liner was tested in a Pi-K demonstration motor (Propulsion Directorate, Air Force Research Laboratory, Edwards, CA). Prior to testing, the liner was wrapped with continuous T-300 carbon fibers (7 μm diameter, Cytec Carbon Fibers LLC, Alpharetta, GA; produced by carbonization of polyacrylonitrile fibers). The fibers were then densified via the *In Situ* Densification process using naphthalene as the matrix precursor [42]. The fiber-wrapped nozzle liner was immersed in naphthalene, which completely infiltrated the voids between the carbon fibers. The

naphthalene was then polymerized *in situ* with the use of an $AlCl_3$ catalyst. The polymerized perform was heated to 1100°C in order to convert the polymer matrix material to carbon. The carbon-carbon composite surrounding the insert was then machined to the final shape required by the test motor. A steel shoulder was adhesively bonded to the carbon-carbon overwrap to enable the nozzle assembly to be held in the Pi-K motor. The completed nozzle was then placed in a Pi-K test motor that had been previously loaded with a solid propellant comprised of 19 wt% aluminum. The propellant grain was ignited and burned for 4.6 s with a maximum pressure of 3.5 MPa.

4. Results and discussion

4.1. Phase and microstructural characterization of DCP-derived composites

Secondary and backscattered electron images of polished cross-sections of a composite generated by the reactive infiltration of Zr_2Cu(l) into a bar-shaped WC preform at 1300°C are shown in Fig. 1a and b, respectively. The WC preform associated with this composite possessed a porosity of 43.5% prior to reactive infiltration. The secondary electron image in Fig. 1a revealed that, after reactive infiltration, the specimen was comprised of a particulate phase encased within a dense matrix. Isolated, fine (<2 μm) pores were detected within the matrix or particulate phases. The higher-magnification backscattered electron image in Fig. 1b revealed that the particles consisted of a grey core and a relatively bright (higher atomic number) coating. The coated particles were enveloped by a darker matrix phase. The matrix phase was found to be enriched in zirconium and carbon by EDX analyses (Fig. 1c), which was consistent with zirconium carbide. EDX analyses (Fig. 1d) revealed that the grey core of the particles was comprised of tungsten and carbon, which was consistent with unreacted tungsten carbide. The composite associated with the images in Fig. 1a and b was generated by exposure

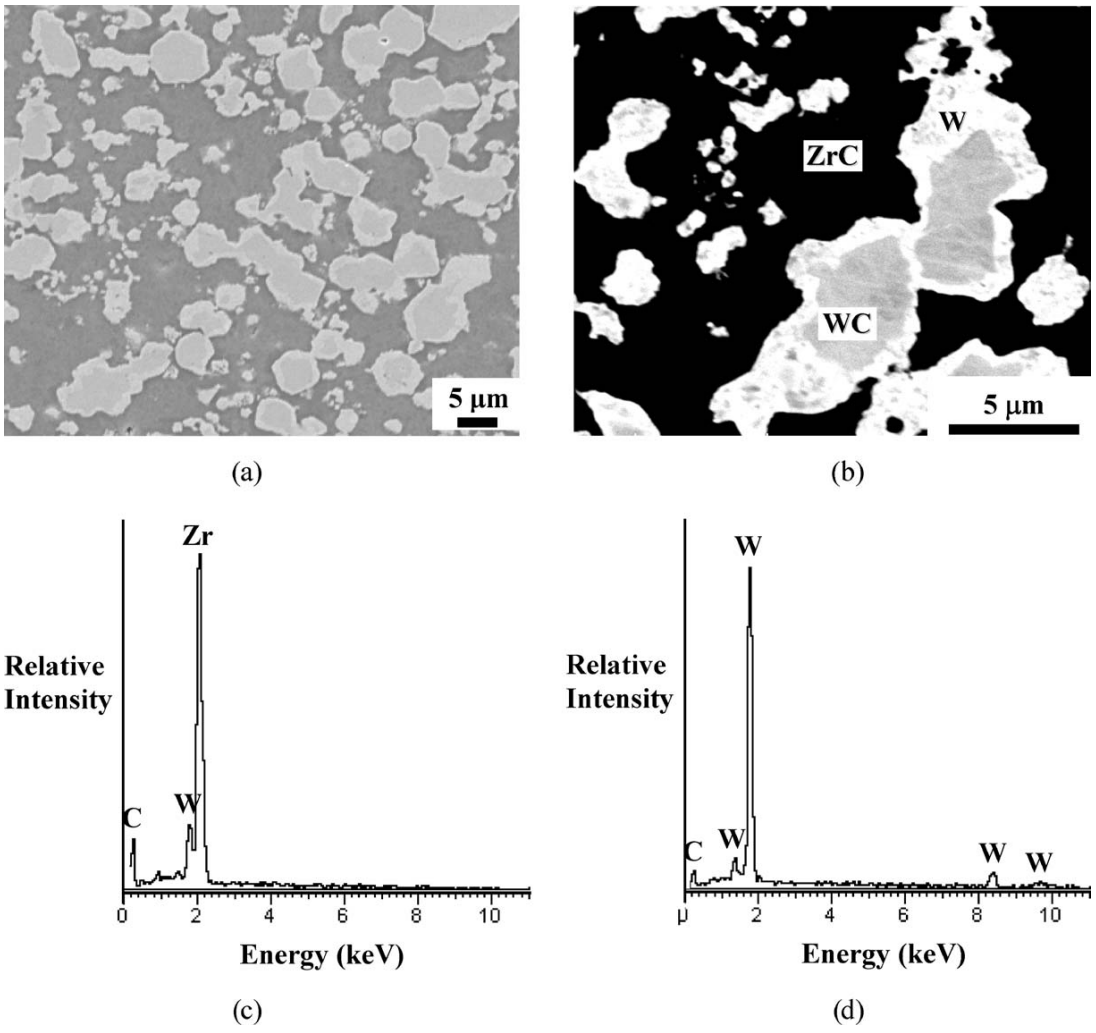

Figure 1 (a) Secondary electron and (b) backscattered electron images of a composite specimen generated by the reactive infiltration of Zr_2Cu(l) into a porous WC preform (43.5 vol% porosity) at 1300°C for 8 h. EDX patterns obtained from the dark matrix phase and the grey core of the particles in (b) are shown in (c) and (d), respectively. (e) Backscattered electron image of a composite specimen generated by the reactive infiltration of Zr_2Cu(l) into porous WC preform (42.4 vol% porosity) at 1300°C for 0.5 h. (f) XRD patterns obtained from WC preforms (46 ± 1% porosity) after infiltration and reaction with Zr_2Cu(l) for 0.5, 2, 4 and 8 h. (g) EDX pattern obtained from an isolated region containing a Cu-rich phase.

(*Continued on next page*.)

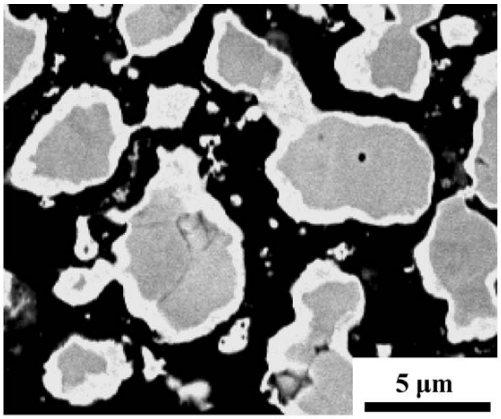

(e)

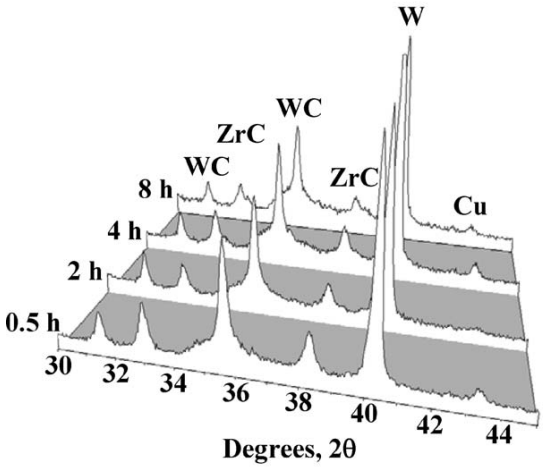

(f)

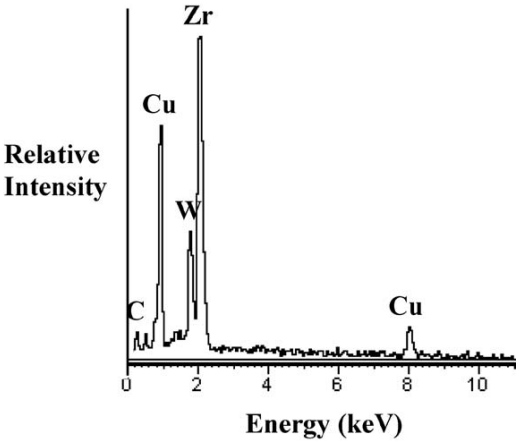

(g)

Figure 1 (*Continued*).

to Zr_2Cu(l) for 8 h. Composites with similar microstructures were also produced after only 0.5 h of exposure of WC preforms of comparable porosity (42.4 vol%) to the Zr_2Cu melt (Fig. 1e). XRD patterns obtained after exposure of WC preforms (with porosities of $46 \pm 1\%$) to the Zr_2Cu melt at 1300°C for various times are shown in Fig. 1f. Distinct diffraction peaks for W, WC, and ZrC were observed. Similar amounts of these phases were detected for reaction times of 0.5 to 8 h [13]. These XRD analyses, along with the EDX analyses in Fig. 1c and d, and the differences in phase contrast observed in the backscattered electron images of Fig. 1b and e, were consistent with composites comprised of tungsten-coated particles of residual (unreacted) tungsten carbide encased within a zirconium carbide-based matrix. A weak diffraction peak for copper was also observed after each reaction time. Small, isolated amounts of a Cu-rich phase (not seen in Fig. 1a, b, and e) were also occasionally detected by EDX analyses (Fig. 1g) in polished composite cross-sections. The weight gain exhibited by a specimen of comparable starting porosity (44.6%) was 32.9%. For the stoichiometry of reaction (1), this weight gain corresponds to a phase content of 23.8 vol% tungsten, 28.4 vol% unreacted tungsten carbide, 38.9 vol% zirconium carbide, and 8.9 vol% copper (or a ZrC + Cu total of 47.8 vol% for the matrix). These values were not far from those obtained by image analyses of backscattered electron images from the specimen shown in Fig. 1a and b: 18.5 ± 2.3 vol% tungsten, 30.9 $\pm$ 6.1 vol% unreacted tungsten carbide, and 50.6 ± 5.4 vol% of the matrix phases (the zirconium carbide and copper-rich phases). (Note: independent evaluation of the amount of the copper-rich phase within the matrix was difficult to obtain by image analyses, owing to the isolated occurrence of this phase, the small contrast difference relative to zirconium carbide, and the fine phase width of <0.2 μm). The phase mixture obtained from the measurement of weight gain possessed a theoretical density of 12.4 g/cm^3. The bulk density measured for a composite specimen generated from a 44.6% porous WC preform was 11.7 g/cm^3, which corresponds to a density of 94.4% (5.6% porosity).

The ZrC matrices and the W coatings on particles observed in the microstructures in Fig. 1a, b, and e were generated within the pore spaces present in the starting WC preforms. The presence of residual WC in these reacted specimens was a result of pore filling prior to complete consumption of the WC. The WC preforms used to generate the composites associated with Fig. 1a–g possessed porosities of 42.4–47.0 vol%. These values of porosity were smaller than what was required to accommodate the internal increase in solid

volume from complete conversion of tungsten carbide into zirconium carbide and tungsten (note: in order to accommodate the 101% increase in internal solid volume due to completion of reaction (1), a target porosity of 50.2 vol% was required [13]). Once the pores become filled, further migration of $Zr_2Cu(l)$ into the preform, and further consumption of WC, were inhibited. The similarities in XRD patterns and microstructures of the specimens generated within 0.5 and 8 h of exposure to $Zr_2Cu(l)$ indicated that the pores were filled, and the reaction was effectively terminated, within 0.5 h at 1300°C.

Secondary electron and backscattered electron images of a polished cross-section of a composite specimen generated by reactive infiltration of $Zr_2Cu(l)$ into a 52.0% porous WC preform are shown in Fig. 2a and b, respectively. The secondary and backscattered electron images reveal a relatively dense specimen, containing a few fine (<2 μm) isolated pores, comprised of a particulate phase contained within a darker matrix. X-ray maps for carbon, zirconium, and tungsten associated with the backscattered electron image in Fig. 2b are shown in Fig. 2c–e, respectively. The matrix phase was enriched in carbon and zirconium, which was consistent with zirconium carbide. The particulate phase was enriched in tungsten and depleted in carbon, which was consistent with metallic tungsten; that is, the particles did not contain residual tungsten carbide. The uniformity in brightness of the particles in the backscattered electron image (i.e., the absence of a relatively bright cladding layer surrounding each particle), and the presence of distinct scratches through the particulate phase (Fig. 2a), were also consistent with particles of relatively soft metallic tungsten in a much harder zirconium carbide matrix. A minor amount of a copper-rich phase (Fig. 2a and f) was also detected by EDX analyses (Fig. 2g). XRD analysis of this specimen (Fig. 2h) revealed peaks for zirconium carbide and tungsten, and a weak peak for copper. Distinct peaks for tungsten carbide were not detected. The weight gain exhibited by a specimen with the same starting porosity (52.0%) was 49.0%. For the stoichiometry of reaction (1), this weight gain corresponds to a phase content of 37.2 vol% tungsten, 60.7 vol% zirconium carbide, and 2.1 vol%

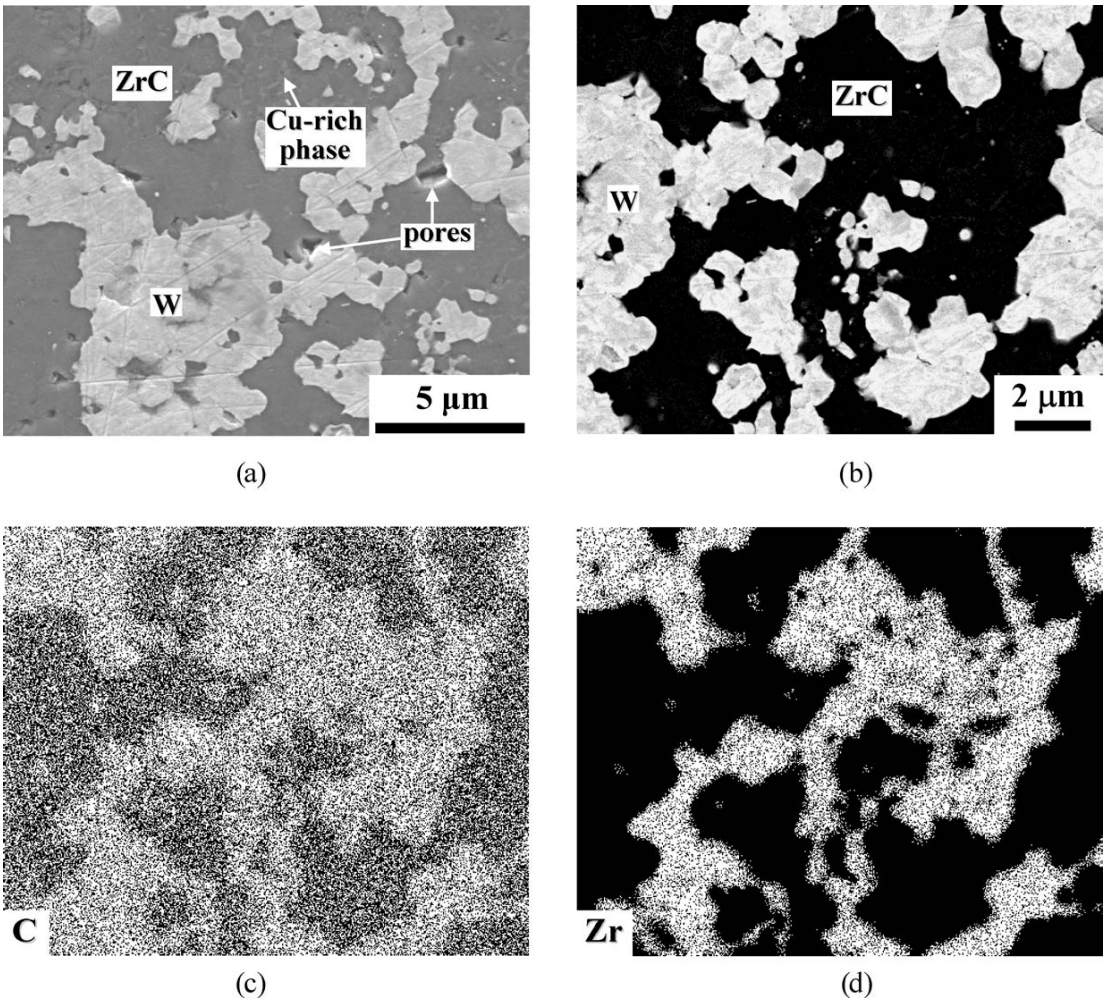

Figure 2 (a) Secondary electron and (b) backscattered electron images of composite specimens fabricate by the reactive infiltration of $Zr_2Cu(l)$ into porous WC preforms (52.0 vol% porosity) at 1300°C. (c) C and (d) Zr X-ray maps associated with the backscattered electron image in (b). (e) W X-ray map associated with the backscattered electron image in (b). (f) Higher magnification secondary electron image of the Cu-rich phase in (a). (g) EDX pattern obtained from the volume containing this Cu-rich phase. (h) XRD pattern obtained from the specimen shown in (a–g).

(*Continued on next page*.)

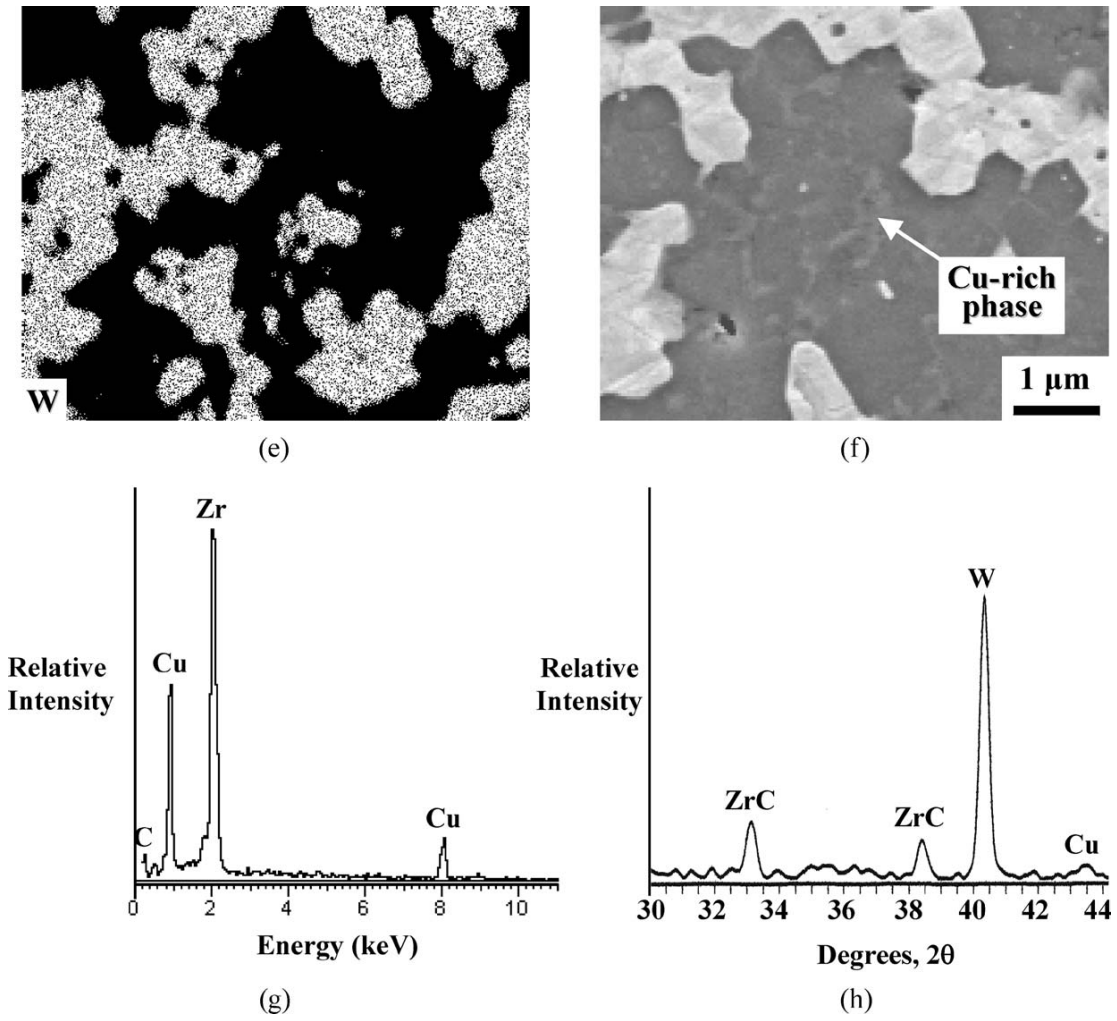

Figure 2 (*Continued*).

copper (or a ZrC + Cu total of 62.8 vol% for the matrix). These values were not far from those obtained by image analyses of backscattered electron images from the specimen shown in Fig. 2a and b: 43.7 ± 6.6 vol% tungsten and 56.3 ± 6.6 vol% of the matrix phases, zirconium carbide and the copper-rich phase. The phase mixture obtained from the measurement of weight gain possessed a theoretical density of 11.4 g/cm^3. The bulk density measured for a composite specimen generated from a 52.0% porous WC preform was 11.0 g/cm^3, which corresponds to a density of 96.5% (3.5% porosity). The enhanced porosity (52.0 vol%) of the starting rigid WC preform for this specimen provided sufficient open volume to enable the WC to be fully consumed just prior to complete filling of the pores.

4.2. Near net-shape fabrication of ZrC/W-based rocket nozzle liners

An optical photograph of a porous, nozzle-shaped WC preform prepared by gel casting followed by a modest sintering treatment (1450°C, 4 h) is shown in Fig. 3a. The geometry of this preform was chosen to be compatible with the Pi-K rocket test discussed below. The bulk density of this preform after light sintering was 7.52 g/cm^3, which corresponded to a porosity of 52.0 vol% (i.e., sufficient for completion of reaction (1)). An optical image of the nozzle insert after reactive infiltration with Zr_2Cu(l) is shown in Fig. 3b. The same specimen is shown in Fig. 3c and d after excess solidified metal adhering to the nozzle surfaces was selectively removed by light polishing (note: the solidified Zr-Cu metal was much softer than the underlying carbide-bearing composite). The weight gain of this nozzle after reactive infiltration was 49.0%, which was not far from that expected (46.6%) for complete conversion of WC into ZrC and W. The nozzle insert retained the shape of the starting porous WC preform. Indeed, the diameters of the entry and exit cones of the nozzle insert changed by ≤0.3 mm after reactive infiltration. The ID of the entry cone changed from 9.63 to 9.65 cm, and the ID of the exit cone changed from 3.02 to 3.05 cm.

4.3. Pi-K rocket test

Prior to rocket testing, the ZrC/W-based insert (Fig. 3) was backed with a carbon-carbon composite. This lightweight C-C composite backing served two functions: (1) to bring the insert to the final external dimensions required for the rocket motor, and (2) to provide

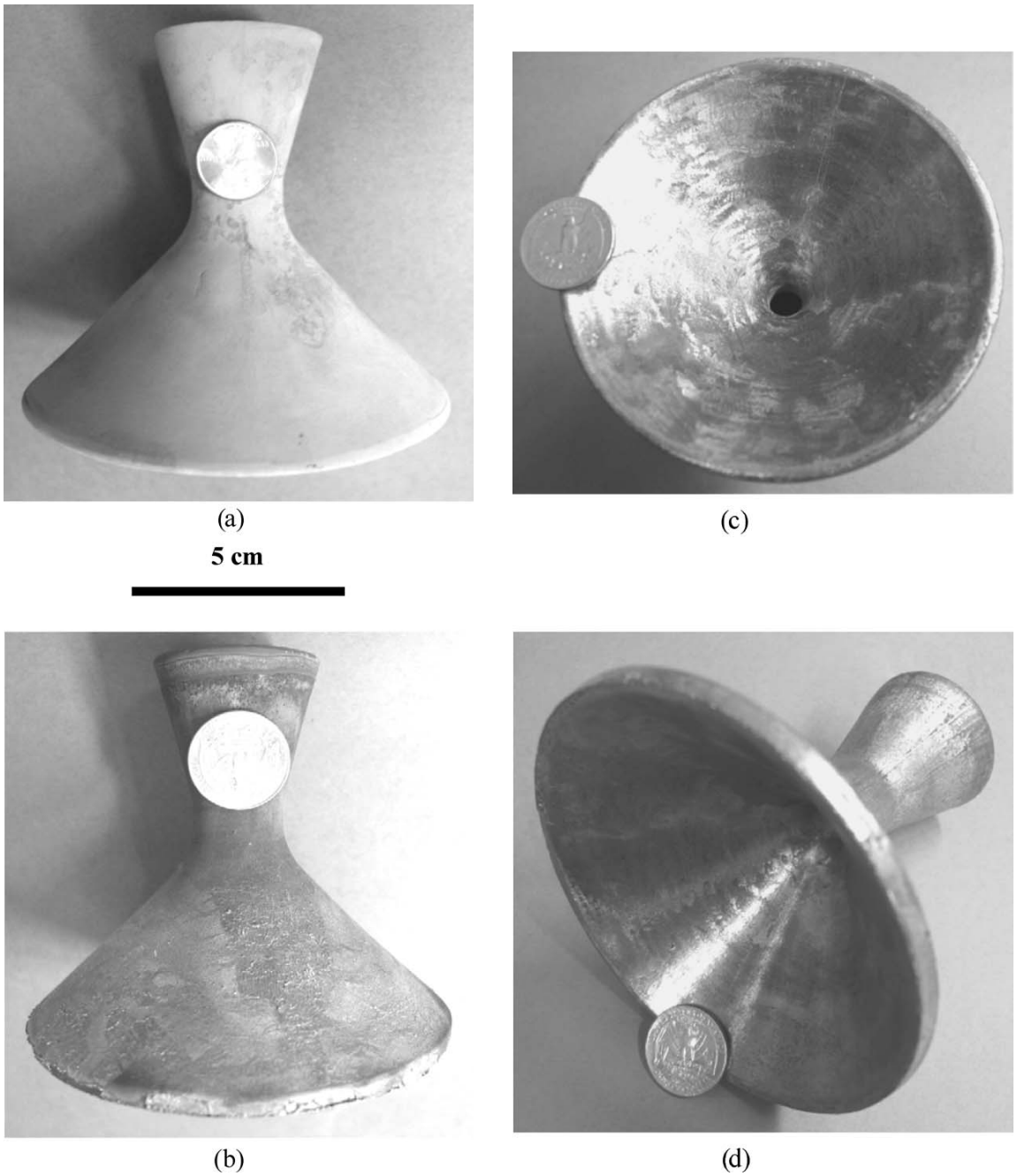

Figure 3 Optical photographs of (a) a nozzle-shaped WC preform (52.0 vol% porosity), and (b) the same specimen after reactive infiltration with Zr_2Cu(l) (immersion for 10 min at 1200°C, followed by heating at 2°C/min to 1300°C), and (c), (d) after removal of the excess solidified metal on the nozzle surfaces by polishing.

mechanical backing to the insert while the interior of the insert was exposed to the high gas pressure during the firing. After machining the C-C backing and bonding a retaining ring to the backing, the completed nozzle (Fig. 4a) was placed in a Pi-K test motor (Fig. 4b), which had been previously loaded with a solid propellant comprised of 19 wt% aluminum. The propellant grain was ignited and burned (Fig. 5a) for 4.6 s with a maximum pressure of 3.5 MPa. The temperature that the throat experienced upon combustion of this propellant was predicted by thermal-chemical calculations to be 3245 K [43]. During the rapid heat up at the start of the test, the pressure within the nozzle increased to a relatively uniform value of about 510 psi (3.5 MPa) (Fig. 5b), which indicated that the nozzle insert survived the critical initial thermal shock associated with rapid heat up. Examination of the nozzle insert after the test indicated that the throat of the nozzle had remained intact. The exit side of the nozzle throat is shown in Fig. 6, where some solidified alumina deposit can be seen. Although the internal surfaces of the insert appeared to be unaffected by the firing (i.e., roughening or recession of the surface was not observed), hairline compression cracks formed on the entrance end of the insert. Such cracking is likely to have resulted from the difference in thermal expansion between the ZrC/W-based insert and

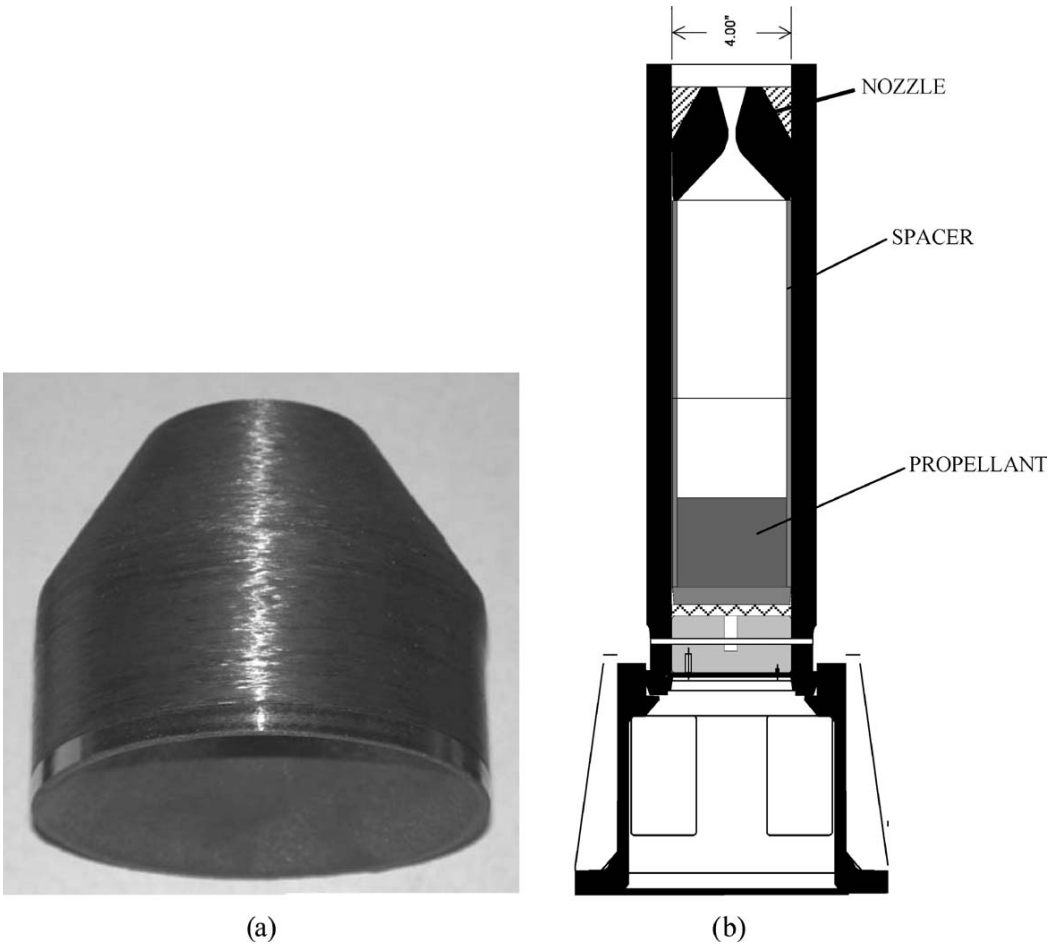

Figure 4 (a) ZrC/W nozzle insert after it had been wrapped with carbon fibers, infiltrated with naphthalene, polymerized, fired (1100°C) to form a C-C composite backing, and machined to size for the test motor. (b) Schematic of Pi-K test motor.

the carbon-carbon backing. Indeed, a distinct cracking sound was heard about 3.3 s from the start of the firing that coincided with the small perturbation seen in the pressure trace in Fig. 5b. Such cracking may be avoided with the use of a compliant layer between the insert and the carbon-carbon backing. In any event, the absence of solidified alumina at the interface of the carbon-carbon backing with the ZrC/W-based insert, or within the hairline cracks in the insert, at the nozzle entrance indicated that appreciable penetration of the combustion products to the carbon-carbon backing did not occur. Although more extensive testing needs to be conducted, the present work indicates that the nozzle insert survived the extreme thermal shock and erosion of the Pi-K test.

Although the present work has focused on the ZrC/W-based composites for rocket nozzles, the DCP process is not limited to these compositions or to this application. Complex-shaped composites containing a variety of other ceramic phases (carbides, borides, nitrides, oxides, etc.) and refractory metals may also be produced for use in a wide range of other high-temperature aerospace (combustion liners, valves, leading edges, exhaust flaps, etc.) and other applications (e.g., erosion-resistant dies for extrusion, drawing, pressing or forming; wear-resistant plates for brakes, skids, or runners; stiff, creep-resistant structural components; hard, lightweight armor) [27, 28].

5. Conclusions

Near net-shaped composites containing the ultra-high-melting phases, zirconium carbide and tungsten, were fabricated at modest temperatures and at ambient pressure by the Displacive Compensation of Porosity (DCP) method. Porous, gel-cast WC preforms in the shape of an hourglass (for rocket nozzle liners) were infiltrated at only 1200–1300°C with molten Zr_2Cu. The zirconium in the liquid displaced the carbon from tungsten carbide to form zirconium carbide and metallic tungsten. Because these latter solid products (ZrC, W) possessed twice the volume of tungsten carbide, the prior pores within the preform became filled by these solid products ("displacive compensation of porosity") and excess liquid was squeezed back out of the preform. Since the WC preform remained rigid during the course of reaction, the external shape and dimensions of the starting preform were preserved in the final nozzle-shaped composite. A DCP-derived, ZrC/W-based nozzle insert backed with a carbon-carbon composite was found to be resistant to the thermal shock and erosive conditions of a solid-fueled Pi-K rocket test. This work

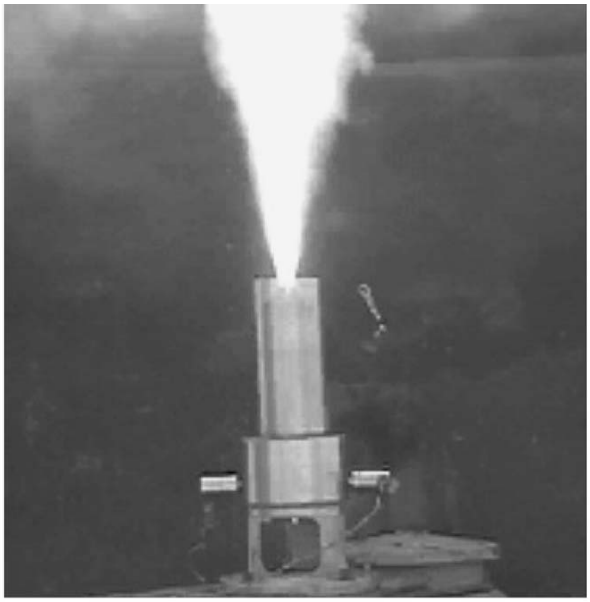

(a)

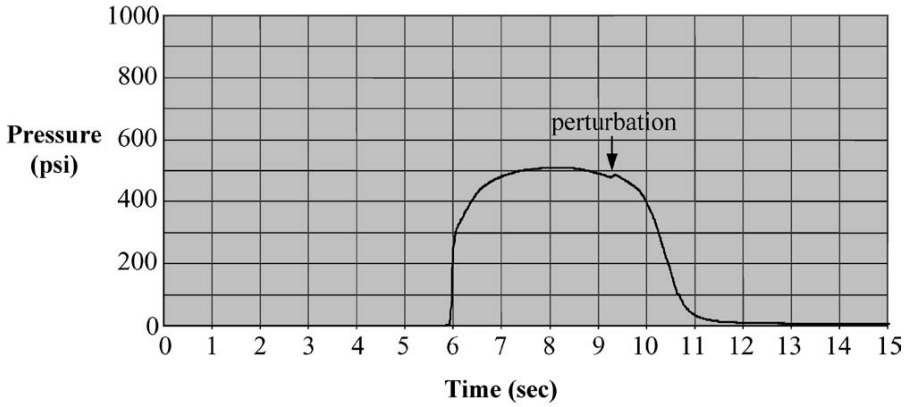

(b)

Figure 5 (a) Test firing of Pi-K motor with carbon-carbon backed ZrC/W insert. (b) Pressure trace during test firing (the perturbation indicated in the pressure trace coincided with a distinct cracking sound).

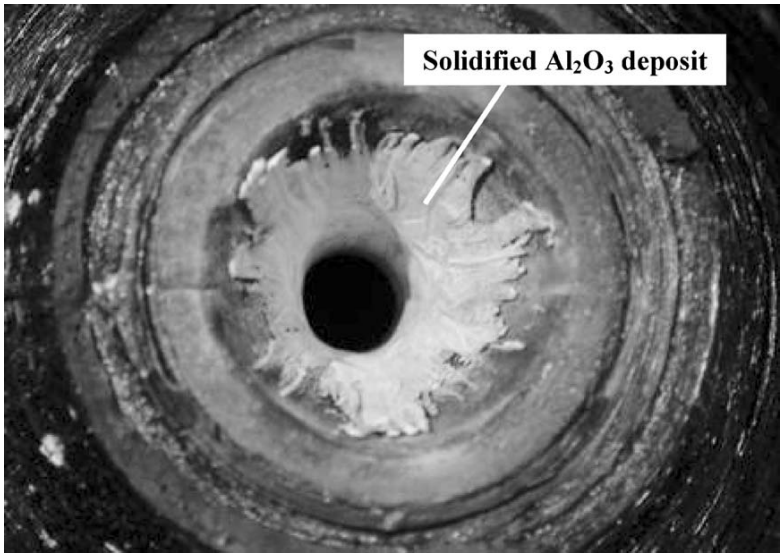

Figure 6 Exit of tested nozzle showing the aluminum oxide deposit on the surface of the ZrC/W insert that is surrounded by the carbon-carbon composite.

demonstrates that the DCP process may be used to fabricate dense, ultra-high-melting, erosion-resistant ceramic/refractory metal composites in complex and near net shapes without the need for high pressure or high temperature densification or extensive machining.

Acknowledgements

This research was supported by the Air Force Office of Scientific Research via Grant No. F49620-02-1-0349 (Dr. Joan Fuller, Program Manager). The technical support of Mr. Hieu Nguyen in conducting the Pi-K test is also gratefully acknowledged.

References

1. K. UPADHYA, in "High Performance High Temperature Materials for Rocket Engines and Space Environment," edited by K. Upadhya (ASM, Materials Park, OH, 1993) p. 1.
2. K. UPADHYA, J. M. YANG and W. P. HOFFMAN, *Amer. Ceram. Soc. Bull.* **76**(12) (1997) 51.
3. G. P. SUTTON, "Rocket Propulsion Elements" (John Wiley and Sons, Inc., New York, NY, 1992) p. 483.
4. E. G. KENDALL and J. D. MCCLELLAND, *Amer. Soc. Testing Mater. Spec. Tech. Publ.* (379) (1964) 71.
5. J. D. WALTON, JR. and C. R. MASSON, JR., *Corrosion* **16** (1960) 371.
6. M. E. DE MORTON, *Wear* **41** (1977) 223.
7. A. A. VICARIO, JR., W. T. FREEMAN, JR. and E. D. CASSEDAY, *J. Spacecraft* **11**(9) (1974) 631.
8. R. C. ROSSI, *Mater. Sci. Res.* **5** (1971) 123.
9. P. R. SUBRAMANIAN and D. E. LAUGHLIN, in "Phase Diagrams of Binary Tungsten Alloys," edited by S. V. Nagender Naidu and P. Rama Rao (Indian Institute of Metals, Calcutta, 1991) p. 76.
10. E. LASSNER and W. D. SCHUBERT, "Tungsten: Properties, Chemistry, and Technology of the Element, Alloys, and Chemical Compounds" (Plenum Publishers, New York, NY, 1999) p. 13, 16, 302.
11. S. W. YIH and C. T. WANG, "Tungsten: Sources, Metallurgy, Properties, and Applications" (Plenum Press, New York, NY, 1979) p. 249, 358, 405.
12. S.HSU, C. CHEN, L. SHEN and K. W. FRANZ, *J. Spacecraft* **14**(4) (1977) 207.
13. "JCPDS X-ray Diffraction Card File" (International Centre for Diffraction Data, ICDD, Newton Square, PA, 1981) Cards No. 4-806 (W), 25-1047 (WC), 35-784 (ZrC), 4-836 (Cu), 18-466 (Zr_2Cu).
14. Metals Handbook, 9th ed., "Properties and Selection: Stainless Steels, Tool Materials and Special-Purpose Metals" (American Society for Metals, Metals Park, OH, 1980) Vol. 3, p. 328.
15. W. D. KLOPP and W. R. WITZKE, *J. Less-Comm. Met.* **24** (1971) 427.
16. K. S. SHIN, A. LUO, B.-L. CHEN and D. L. JACOBSON, *J. Metals* **42**(8) (1998) 12.
17. E. K. STORMS, "The Refractory Carbides" (Academic Press, New York, NY, 1967) p. 18.
18. W. S. WILLIAMS, in "Progress in Solid State Chemistry," edited by H. Reiss and J. O. McCaldin (Pergamin Press, New York, NY, 1971) p. 57.
19. Phase Equilibria Diagrams, "Borides, Carbides, and Nitrides", edited by A. E. McHale (The American Ceramic Society, Westerville, OH, 1994) Vol. X, p. 371.
20. Y. S. TOULOUKIAN, R. K. KIRBY, R. E. TAYLOR and P. D. DESAI, "Thermophysical Properties of Matter, Vol. 12: Thermal Expansion of Metallic Elements and Alloys" (Plenum Press, New York, NY, 1975) p. 354.
21. Y. S. TOULOUKIAN, R. K. KIRBY, R. E. TAYLOR and T. Y. R. LEE, "Thermophysical Properties of Matter, Vol. 13: Thermal Expansion of Nonmetallic Solids" (Plenum Press, New York, NY, 1977) p. 926.
22. Y. S. TOULOUKIAN, R. W. POWELL, C. Y. HO and P. G. KLEMENS, "Thermophysical Properties of Matter, Vol. 1: Thermal Conductivity of Metallic Elements and Alloys" (Plenum Press, New York, NY, 1970) p. 428.
23. *Idem*., "Thermophysical Properties of Matter, Vol. 2: Thermal Conductivity of Nonmetallic Solids" (Plenum Press, New York, NY, 1970) p. 611.
24. G. M. SONG, Y. J. WANG and Y. ZHOU, *J. Mater. Sci.* **36** (2001) 4625.
25. *Idem*., *Mater. Sci. Eng.* A **A334** (2002) 223.
26. G. M. SONG, Y. ZHOU, Y. J. WANG and T. C. LEI, *J. Mater. Sci. Lett.* **17** (1998) 1739.
27. K. H. SANDHAGE, R. R. UNOCIC, M. B. DICKERSON, M. TIMBERLAKE and K. GUERRA, "Method for Fabricating High-Melting, Wear-Resistant Ceramics and Ceramic Composites at Low Temperatures," U.S. Patent No. 6,598,656, July 29, 2003.
28. K. H. SANDHAGE and P. KUMAR, "Method for Fabricating Shaped Monolithic Ceramics and Ceramic Composites Through Displacive Compensation of Porosity, and Ceramics and Composites made Thereby," U.S. Patent No. 6,407,022, June 18, 2002.
29. P. J. WURM, P. KUMAR, K. D. RALSTON, M. J. MILLS and K. H. SANDHAGE, in "Innovative Processing and Synthesis of Ceramics, Glasses, and Composites V. Ceram. Trans.," edited by J. P. Singh, N. P. Bansal, A. Bandyopadhyay, and L. Klein (The American Ceramic Society, Westerville, OH, 2002) Vol. 129, p. 93.
30. P. KUMAR, N. A. TRAVITSKY, P. BEYER, K. H. SANDHAGE, R. JANSSEN and N. CLAUSSEN, *Scripta Mater.* **44**(5) (2001) 751.
31. P. KUMAR and K. H. SANDHAGE, *J. Mater. Sci.* **34**(23) (1999) 5757.
32. P. KUMAR, S. A. DREGIA and K. H. SANDHAGE, *J. Mater. Res.* **14**(8) (1999) 3312.
33. K. A. ROGERS, P. KUMAR, R. CITAK and K. H. SANDHAGE, *J. Amer. Ceram. Soc.* **82**(3) (1999) 757.
34. M. B. DICKERSON, R. L. SNYDER and K. H. SANDHAGE, *ibid.* **85**(3) (2002) 730.
35. Z. GRZESIK, M. B. DICKERSON and K. H. SANDHAGE, *J. Mater. Res.* **18**(9) (2003) 2135.
36. I. BARIN, "Thermochemical Data of Pure Substances" (VCH Verlagsgesellschaft, Weinheim, Germany, 1995) p. 1788, 1860.
37. O. J. KLEPPA and S. WATANABE, *Metall. Trans.* B **13B** (1982) 391.
38. N. SAUNDERS, *CALPHAD: Comput. Coupling Phase Diagr. Thermochem.* **9** (1985) 297.
39. E. KNELLER, Y. KHAN and U. GORRES, *Z. Metallkunde* **77**(1) (1986) 43.
40. P. R. SUBRAMANIAN and D. E. LAUGHLIN, in "Phase Diagrams of Binary Copper Alloys," edited by P. R. Subramanian and D. E. Laughlin (ASM International, Materials Park, OH, 1994) p. 109.
41. R. RESNICK, C. WURMS, R. STEINITZ and E. MAZZA, *Metals Eng. Quart.* **3**(2) (1963) 51.
42. P. G. WAPNER, W. P. HOFFMAN and J. P. JONES, U.S. Patent No. 6,309,703, Oct. 30, 2001.
43. C. SELPH, Air Force Research Laboratory, unpublished work.

Received 21 November 2003
and accepted 19 April 2004

APPENDIX B

"Material Science of Carbon"
Handbook of Materials Modeling,
W.P. Hoffman,
S.Yip, Editor, 2923-2928 (2005)

Material Science of Carbon

Carbon is a ubiquitous material that is essential for the functioning of modern society. Because carbon can exist in a multitude of forms, it can be tailored to possess practically any property that might be required for a specific application. The list of applications is very extensive and includes: aircraft brakes, electrodes, high temperature molds, rocket nozzles and exit cones, tires, ink, nuclear reactors and fuel particles, filters, prosthetics, batteries and fuel cells, airplanes, and sporting equipment.

The different forms of carbon arise from the fact that carbon exists in three very different crystalline forms (allotropes) with a variety of crystallite sizes, different degrees of purity and density, as well as various degrees of crystalline perfection. These allotropes are possible because carbon has four valence electrons and is able to form different kinds of bonds with other carbon atoms.

For example, diamond with a covalently-bonded face-centered cubic structure can exist as a naturally–formed single crystal as large as 200 g. Diamond, the hardest material known to man, is also able to be made synthetically by a variety of processes. For example, high pressure anvils can be utilized to produce relatively small single crystals while a vapor-phase process such as chemical vapor deposition (CVD) is employed to deposit crystalline and amorphous coatings having grain sizes on the micron scale, and a variety of degrees of crystallite orientations. Synthetic diamonds in all forms are used as hard scratch-resistant coatings and tool coatings for grinding, cutting, drilling and wire drawing. Other applications include heat sinks and optical windows among others.

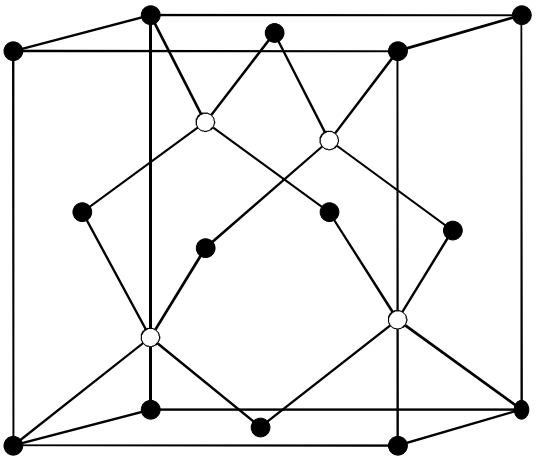

Diamond Structure

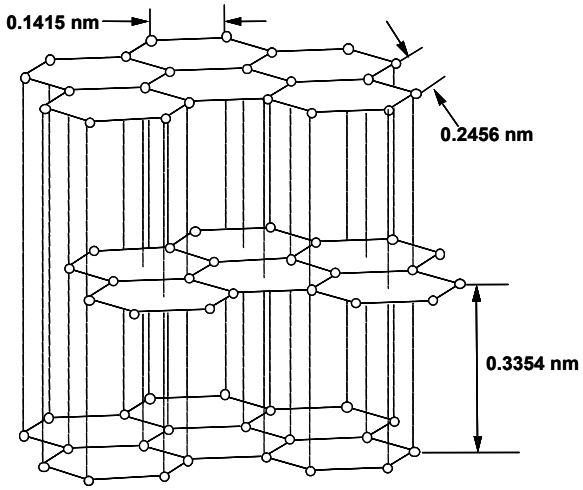

Hexagonal Graphite Structure

The most abundant forms of carbon exist as various forms of the allotrope hexagonal graphite. The perfect crystalline structure of graphite is a hexagonal layered structure in which the atoms in each layer are covalently-bonded while the graphene layers are held together by weaker Van Der Waals forces. This difference in bonding is what is

responsible for the great anisotropy in mechanical, thermal, electrical and electronic properties.

With the relatively recent discovery of the nano-forms of carbon in the last two decades, the range of properties that carbon can possess and the gamut of potential applications has greatly increased. The linear portions of these molecules are simply rolled up graphene layers, while the curved portions consist of graphite hexagons in contact with pentagons. Although commercial applications for both bucky balls and carbon nanotubes are not well defined at the time of this writing, the high aspect ratio of nanotubes, along with the fact that they are stronger (63 GPa) and stiffer (~1000 GPa) than any other known material, means that the potential for these materials is great.

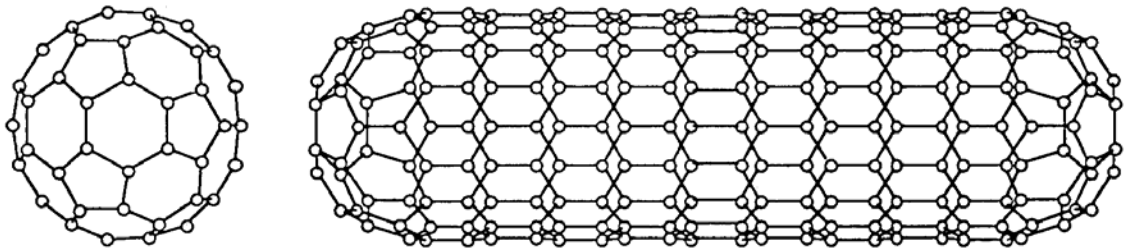

BUCKYBALL **NANOTUBE**

Adding to the complexity of understanding and modeling carbon is the fact that, in its various forms, it rarely exists in a perfect single crystalline state. For example, perfect graphitic structure only exists in the various forms of natural graphite flakes and graphitizable carbons, which are carbons formed from a gas or liquid phase process. An example of a graphitizable carbon would be highly oriented pyrolytic graphite (HOPG), which is formed by depositing one atom at a time on a surface utilizing the pyrolysis of a hydrocarbon, such as methane or propylene. This deposited material is then graphitized employing both thermal and mechanical stress.

In the overwhelming number of applications, single crystal graphite is not employed. Rather a carbon with some degree of graphite structure is utilized. Excluding crystallite imperfection, such as vacancies, interstitials, substitutions, twin planes, etc., the form of carbon that most closely approaches single crystal graphite is turbostratic graphite. This form of carbon looks very similar to graphite except that, although there may be some degree of perfection within the planes, the adjacent planes are out of registry with one another. That is, in the hexagonal graphite structure, there is an atom in each adjacent plane that sits directly over the center of the hexagonal ring. In turbostratic graphite, the adjacent planes are shifted with respect to one another and are out of registry. This results in an increase in the interlayer spacing, which can increase from 0.3354 nm to more than 0.345 nm. If the value exceeds this, the structure exfoliates. Heating to temperatures in excess of 2800 K provides energy for mobility and can convert turbostratic graphite to single crystal graphite in a process called graphitization.

As stated above, a carbon material that goes through either a gas phase or liquid phase process in its conversion to carbon (carbonization process) can be converted to a graphitic structure employing time and temperature in the range from 2000-2800 K. This means that materials formed in the gas phase (like carbon black and pyrolytic carbon) can be converted to a graphitic structure. Cokes and carbon fibers fabricated from petroleum, coal tar, or mesophase pitch are also graphitizable. On the other hand, chars formed directly from organic materials, such as wood and bone used for activated carbon, PAN fibers formed from polyacrylonitrile, and vitreous carbons formed from polymers, such as phenolic or phenyl-formaldehyde, are amorphous and not graphitizable because they maintain the same rigid non-aligned structure that they possessed before carbonization.

In addition to the degree of crystalline order, the properties of carbons are also determined by the crystallite size and orientation of polycrystalline carbons. The largest carbon parts that are manufactured are electrodes for the steel and aluminum industries. These electrodes can weigh more than 3 tons and are fabricated by extruding a mixture of fine petroleum coke and coal tar pitch. The extrusion process causes some preferential alignment of the crystallites, and baking to 2800 K produces a polycrystalline graphite part that has high strength and conductivity. To make isotropic graphite, fine-grain coke and petroleum pitch are isostatically pressed.

By proper selection of precursor material and processing condition, a carbon with practically any property can be produced. For example carbons can be hard (chars) or soft (blacks), strong (PAN fibers) or weak (aerogel), stiff (pitch fibers) or flexible (Graphoil®), as well as anisotropic (HOPG) or isotropic (polycrystalline graphite). In addition, porosity, lubricity, hydrophobicity, hydrophilicity, thermal conductivity and surface area can be varied over a wide range. For example, surface area can vary from 0.5 m^2/g for a fiber to > 2000 m^2/g for an activated carbon, while thermal conductivity can range from 0.001 W/(m-K) for an amorphous carbon foam to 1100 W/(m-K) for a pitch fiber, and 3000 W/(m-K) for diamond.

Carbon materials have been studied and produced for thousands of years. (The Chinese used lampblack 5000 years ago.) While much is understood about carbon, there are some very important areas in which there is still a lack of understanding. These areas fall generally into the production of graphitic material and the oxidation protection of carbon and graphite materials. A better understanding of the science of carbon formation will allow increased performance at reduced cost, while effective oxidation protection at ultra high temperature will enable a whole range of new technology.

Currently, the highest performance and highest cost form of carbon are carbon-carbon composites, which are truly a unique class of materials. These composites, which are stronger and stiffer than steel as well as being lighter than aluminum, are currently used principally in high performance-high value applications in the aerospace and astronautics industries. The highest volume of carbon-carbon is used as brake rotors and stators for military and commercial aircraft because it has high thermal conductivity, good frictional properties, and low wear. Astronautic applications include, rocket nozzles, exit cones,

and nose tips for solid rocket boosters as well as leading edges and engine inlets for hypersonic vehicles. In these applications carbon-carbon's high strength and stiffness as well as its thermal shock resistant are keys to its success. For re-useable hypersonic vehicles, the fact that carbon does not go through phase changes like some ceramics and in fact its mechanical properties actually increase with temperature make this a very valuable material. For satellite applications carbon-carbon's high specific strength and stiffness as well as its near zero thermal expansion make it an ideal material for large structures that require dimensional stability as they circle the earth.

Carbon-carbon composites are fabricated through a multi-step process. First, carbon fibers, which carry the mechanical load, are woven, braided, felted, or filament wound into a preform which has the shape of the desired part. The perform is then densified with a carbon matrix, which fills the space between the fibers and distributes the load among the fibers.

It is this densification process that is not well understood. Unlike the manufacture of fiberglass, in the formation of carbon-carbon composites the matrix precursor is not just cured but must be converted into carbon. The conversion of polymers to produce a char, as well as the conversion of a hydrocarbon gas to produce a graphitizable matrix, is fairly well understood. What is not clear is the process of converting a pitch-based material to a high quality graphitizable matrix. That is, for example, starting with a petroleum or coal tar pitch, heat soaking converts this isotropic mixture of polyaromatics into anisotropic liquid crystalline spherical droplets called mesophase spherules. These spherules ultimately coalesce to form a continuous second phase which ultimately pyrolyzes to form a graphitic structure. Although this process has been observed microscopically, little is known about the process, or even exactly what mesophase is or what molecular precursors are needed to form mesophase. Little is known because it has proved impossible to accurate analyze mesophase precursors, mesophase itself, or the intermediates between mesophase and graphite. What is needed is a model that can predict the growth of single aromatic rings through the mesophase intermediate and into an ordered graphitic structure.

Moreover, it is well known that during pyrolysis, mesophase converts into a matrix that is very anisotropic. The formation of onion-like "sheaths" takes place on the surface of individual carbon fibers in the carbon composite. As these sheaths grow outward from the fiber surfaces, they ultimately collide, forming point defects called disclinations. This behavior has a pronounced effect on both the chemical and physical properties of the carbon-carbon composite. A model that describes this matrix contribution to the composite's properties would be of great benefit for understanding experimental data, such as thermal conductivity and mechanical properties, as well as for prediction of composite behavior.

Although carbon-carbon composites possess high strength, stiffness, and thermal shock resistance, making them an excellent high temperature structural material, their Achilles heel is oxidation. Above 670 K, carbon oxidizes. This means that if it is unprotected, it cannot be used for long-term high temperature applications. Today it is used for short-

term applications, such as aircraft brakes, as well as rocket nozzles, exit cone, and nose tips. To be used in long-term applications such as reusable hypersonic vehicles, it must be protected. Currently, an adequate protection system at ultra high temperatures (>2700 K) does not exist. There is a tremendous need and payoff for a non-structural barrier that can keep oxygen from reaching a carbon surface at 2700 K. Efforts to fabricate these coatings have been unsuccessful. What is probably required for success is some sort of novel functionally graded coating which will require modeling material properties as well as thermal stresses.

Finally, the rather recent discovery of Buckyballs and nanotubes, which are three-dimensional analogs of hexagonal graphite, has also rekindled the need for models of the intercalation of graphite. This process occurs when various elements, such as lithium, sodium, or bromine, "sandwich" themselves between graphene planes. This greatly alters the thermal and electrical properties of the graphite. Similar behavior is beginning to be demonstrated in Buckyballs and nanotubes. The need for models based on computational chemistry would be of great help in this area.

For additional information on carbon, there are many good reference works. Most focus on specific forms of carbon such as carbon blacks, active carbons, fiber, composites, intercalation compounds, nuclear graphites, etc. For general topics the handbook by Pierson (Pierson, 1993) is a good text. A reference work covering scores of subjects in great detail is the 28 Volume Chemistry and Physics of Carbon (Radovic, 2001) which has had three Editors over the last 39 years.

Wesley P. Hoffman
Air Force Research Laboratory
Edwards CA USA

wesley.hoffman@edwards.af.mil

Bibliography

Pierson, H.O., 1993. *Handbook of Carbon, Graphite, Diamond and Fullerenes - Properties, Processing and Applications***.** Noyes Punlications, Park Ridge

Walker P.L. Jr., P Thrower P., and Radovic L.R. (eds) *Chemistry and Physics of Carbon* , Vol. 1-28, Marcel Decker, New York

APPENDIX C

"**Microstructural Studies of In-Situ Mesophase Transformation in the Fabrication of Carbon-Carbon Composites**"

K. M. Chioujones, W. Ho, P. C. Chau, B. Fathollahi,
P. G. Wapner, and W. P. Hoffman,
Carbon, **44**, 284 (2006)

Available online at www.sciencedirect.com
SCIENCE DIRECT®
Carbon 44 (2006) 284–292
CARBON
www.elsevier.com/locate/carbon

Microstructural analysis of in situ mesophase transformation in the fabrication of carbon–carbon composites

K.M. Chioujones [a], W. Ho [a], B. Fathollahi [a,*], P.C. Chau [a], P.G. Wapner [b], W.P. Hoffman [c]

[a] Chemical Engineering Program, University of California, San Diego, La Jolla CA 92093-0411, United States
[b] ERC Inc., 10 East Saturn BLVD, Edwards, CA 93524, United States
[c] Air Force Research Laboratory, 10 East Saturn BLVD, Edwards, CA 93524, United States

Received 25 May 2005; accepted 20 July 2005
Available online 31 August 2005

Abstract

In this work, we examined the microstructures formed during the pyrolysis of naphthalene mixed with $AlCl_3$ catalyst, in the critical temperature range of 300–500 °C and at varying pressures. In addition, non-rigidized preforms were densified by multiple cycle in situ transformation and compared the process with impregnation using fully transformed AR mesophase pitch under similar conditions. The process of mesophase formation in the bulk phase and within tightly packed fiber bundles was observed to be similar: spherule nucleation from the isotropic phase, coalescence of spherules forming bulk mesophase, and mesophase flow before hardening. The hardened mesophase displays the coarse, fibrous, and lamellar microstructure observed in needle cokes. The molten naphthalene was observed to evenly penetrate in-depth the large void spaces and fiber bundles. After two in situ cycles, the fiber bundles and the inter-fiber bundle regions were well filled with transformed mesophase. The incremental filling of the larger void spaces reduced the calculated filling efficiencies from 47% in the first cycle to below 15% in the third through fifth cycle. An 8% improvement in densification efficiencies was achieved by applying modest pressures during the pyrolysis. The extent of mesophase penetration with AR mesophase was observed to decrease from the outer to the inner regions of the preform. The results suggest impregnation with naphthalene catalyst mixture is efficient in filling tightly packed fiber bundles but not large void spaces. Multiple cycles are required in order to fill the large void spaces.

Keywords: Carbon composite, Mesophase; Microstructure; Optical microscopy

1. Introduction

Injection of a low viscosity, fully transformed mesophase pitch into a fiber preform is an effective approach to fabrication of advanced, high-performance carbon–carbon (C/C) composites [1]. Here, flow-induced microstructures can be stabilized by oxidation such that upon carbonization, the fibrous carbon needles running through the flow channels are retained. Using the injection and stabilization process, one can raise the density of C/C composites to reasonably high levels in a couple of cycles.

While the injection method is effective in making highly densified materials with controlled microstructure, it is not without constraints. This method is best applied to uniform geometries such as aircraft brakes, and the use of rigidized preforms is required to resist compaction under injection pressure. Severe injection conditions with diminishing return in density gain could be encountered if the process has to be carried beyond two to three cycles.

* Corresponding author. Tel.: +1 858 5342569; fax: +1 858 53444543.
E-mail address: bfatholl@ucsd.edu (B. Fathollahi).

0008-6223/$ - see front matter © 2005 Elsevier Ltd. All rights reserved.
doi:10.1016/j.carbon.2005.07.026

For non-uniform geometries such as nozzle cones that are not amendable to injection or a vacuum process, an efficient and low-cost impregnation process is needed to densify a C/C composite in multiple cycles. The selection of a matrix precursor having the ideal properties of low viscosity, good wettability, and high carbon yield is essential for efficient densification [2,3]. In practice, however, one generally needs to seek a compromise to reach a final composite density. A low viscosity precursor with the ability to wet carbon fibers can result in uniform density and effectively fill fine pores and cracks in subsequent impregnation cycles, but such a precursor tends to have lower carbon yield. The carbon yield can be improved by applying high-pressure pyrolysis and carbonization with high cost equipment. Alternatively, a precursor with high carbon yield, such as partially or fully transformed carbonaceous mesophase, will reduce the number of impregnation cycles, but in this case, the viscosity of the precursor may not be sufficiently low.

Based on the in situ mesophase transformation of a very low viscosity precursor, the Air Force Research Laboratory has developed a rapid, low cost impregnation process that can be applied at ambient pressure for densification of C/C composites [4]. The Air Force method is based on the mesophase pitch synthesis process advanced by Mochida et al. [5–8]. They used controlled catalytic polymerization of pure aromatic hydrocarbons such as naphthalene to produce a low-viscosity liquid phase that is further transformed into mesophase with good control of the softening point. Their work is also the basis of the commercially available AR mesophase pitches that have been utilized for spinning filaments, injection of brake preforms, and in fabrication of anode materials for lithium ion batteries.

The principle behind the impregnation with in situ transformation process is that a wetting molten monomer can easily penetrate a fiber bundle or void space in a preform by capillary forces. Once the preform is completely filled, in situ polymerization leads to formation of mesophase. Pyrolysis gases tend to blow bubbles and exude carbon matrix from the larger voids. However, the mesophase formed within the fiber bundles and small pores are, to the most part, retained after pyrolysis. Even so, this impregnation and in situ transformation approach will require more processing cycles than injection processes. On the other hand, this is an acceptable trade-off when one considers the relative ease and quickness of impregnation cycles.

In this work, we explored the evolution of microstructures at various stages during mesophase formation to better understand the transformation and impregnation with a wetting monomer and catalyst mixture. As an extension to the series of works by Mochida et al. [5–7], we have also investigated multiple cycle in situ transformation and compared the process with impregnation using fully transformed AR mesophase pitch under similar conditions. Naphthalene was the precursor monomer, and aluminum chloride was chosen as the catalyst. Even though $AlCl_3$ may be retained in the final composite product, we consider its use as a much more environmentally benign alternative to using HF/BF_3. If the amount of $AlCl_3$ is chosen appropriately, there should be minimal impact on the final composite functionality. The microstructures of mesophase formation in bulk and within preforms were examined at various stages in temperature ranges critical to mesophase formation and hardening.

2. Experimental methods

To study the microstructures formed during mesophase transformation, the bulk phase pyrolysis experiments followed the approach described by White and co-workers [9,10]. All transformation and impregnation runs were carried out in a pyrolysis chamber consisting of a cylindrical aluminum block with four slots machined precisely for tight fitting of aluminum test tubes (19 mm × 102 mm). The aluminum tubes were enclosed within the chamber with narrow gas ports to provide a continuous purge stream of nitrogen and to limit the return of volatilized material during pyrolysis. The entire chamber was wrapped in a clamp-shell heater and insulating material, but in a design that facilitated expedient intermittent sample removal.

In each run, 10 g of naphthalene (Aldrich Chemicals, 99% purity, Cat. No. 147141) was mixed relatively quickly with 5 wt.% $AlCl_3$ (Aldrich Chemicals, 99% purity, Cat. No. 237051) in a mortar before being placed in the aluminum tubes. For microstructural studies of the early stages of in situ mesophase transformation within a preform, a small rectangular piece of CVI-rigidized non-woven preform (about 7.5 mm × 7.5 mm × 15 mm or 18 mm × 18 mm × 15 mm) excised with a diamond cutter was also placed in the tube such that it was submerged once the naphthalene had melted. The non-woven preform consisted of 34 mat plies of PAN-based fibers that are laid up in a regular rotational pattern from ply to ply. The volume fraction of the non-rigidized preform was 28%. The filaments were coated with carbon by CVI to a thickness of about 3 μm. In subsequent multicycle densification studies, a non-rigidized preform with fiber volume fraction of 26% was used. The overall preform architecture is governed collectively by the organization of fiber bundles, the inter-fiber bundle regions, and the principal void space among the bundles.

The temperature of the chamber was raised rapidly from room temperature to 100 °C at a rate of about 230 °C/h. From here, the temperature was raised with a constant ramp varying between 30 and 80 °C/h to the desired set point, which ranged from 300 to

480 °C, at which point the temperature was held constant for various periods up to 3 h. In multi-cycle densification experiments using non-rigidized preforms, the temperature was also kept constant for 0.5 h at 100 °C before starting the temperature ramp in order to allow in-depth penetration of naphthalene. The chamber was sealed at the top and pressurized with nitrogen in the pyrolysis experiments under pressure. The chamber pressure was monitored by a pressure gauge. The temperature was monitored by a K-type thermocouple embedded within the aluminum block and interfaced with the computer using an InstruNet (GW Instruments). Temperature ramping profile was implemented with a control program written in LabView.

Samples were removed at various temperatures and time intervals and quenched at room temperature by inserting the tubes in a second aluminum block with similar size slots. For the bulk phase studies, the entire aluminum tube with its contents was mounted and sectioned to provide a full vertical profile for subsequent polishing. In densification studies, the quenched preform was removed from each aluminum tube and weighed in order to determine the carbon yield after pyrolysis. The microstructures of polished sections were examined by polarized-light micrography.

Impregnation experiments were also performed using the ARA24R mesophase pitch. This mesophase pitch has a softening point of 297 °C and a density of 1.3 g/cm^3 [8]. About 10 g of AR mesophase pitch was placed in a sample tube together with a piece of non-rigidized preform that was submerged once the mesophase had melted. The temperature was raised from room temperature at a heating rate of 110 °C/h to a set point of 350 °C at which point it was held constant for about 2.5 h. The quenched samples were oxidized and carbonized.

Oxidative stabilization was performed at 170 °C and ambient pressure for 25 h in a tube furnace purged with a gentle flow of oxygen [11]. Carbonization of the naphthalene and AR impregnated samples was also carried out in a tube furnace, but under a purging stream of nitrogen. Samples were carbonized at a rate of 60 °C/h starting from 100 to 600 °C and at a rate of 180 °C/h from 600 to 1150 °C. After carbonization, specimens were cut to expose the innermost vertical section and embedded in epoxy before a series of polishing for microscopic analysis.

3. Results and discussion

There is no unique processing procedure leading to the formation of carbonaceous mesophase. Therefore, the following micrographs illustrating the progressive morphological stages are only representative of several selected sets of plausible operating procedures based on previous studies [5–7,9,10].

The gradual in situ mesophase transformation during earlier stages was examined under various heating profiles in CVI-rigidized preforms. In this step, we chose to use rigidized preforms in order to minimize damage to the as-impregnated fragile fiber bundles in the polishing process. The mesophase transformation in the bulk phase is presented first. The evolution of microstructures during transformation within a rigidized preform follows. The results of non-rigidized preform densification in multiple cycles will be addressed last.

3.1. Mesophase transformation in the bulk phase

Overall, the formation of mesophase microstructures starting with naphthalene follows the common pattern of transformation from the polymerization of an isotropic hydrocarbon to nucleation of Brooks-and-Taylor (B–T) spherules, and subsequent coalescence to form bulk mesophase. The pyrolysis of naphthalene in the presence of catalysts leads to formation of dimers, trimers, and higher molecular weight molecules from which B–T spherules precipitates [5–7]. The formation of microstructures at various stages during the pyrolysis of naphthalene to 475 °C at a heating rate of 80 °C/h are shown in Fig. 1. Formation and precipitation of anisotropic mesophase spherules was observed for the sample removed from the chamber upon reaching the temperature of 350 °C and quenched at room temperature (Fig. 1(a)). The mesophase layers are aligned perpendicular to the polar diameter but curved to meet the interface with the isotropic phase at high angle. The spherules had a large size distribution, ranging from a few microns to approximately 50 μm. As pyrolysis proceeded to higher temperatures, the larger spherules were collected at the bottom of the tube and began coalescing to form bulk mesophase. Extensive mesophase deformation caused by bubble percolation was observed with increasing temperature and hold time. At this stage, the viscosity of the transforming fluid was sufficiently low to permit flow and structural rearrangement of the coalescing mesophase. The bubbles, mainly methane and hydrogen, were produced by pyrolysis via dealkylation and dehydrogenation reactions [5–7,12,13].

For the specimen removed at 400 °C, the optical analysis of the polished vertical section indicated a total mesophase conversion of about 95%. The coarse, fibrous, and lamellar microconstituents were clearly evident as illustrated in Fig. 1(b) and (c). The fibrous microstructure was produced by uniaxial stretching, and the lamellar microstructure observed in bubble walls resulted from biaxial deformation during growth of gas bubbles [14]. Islands of untransformed isotropic phase containing small number of mesophase spherules were observed deep within bulk mesophase (Fig. 1(b)). Eventually, the flow of bulk mesophase due to bubble percolation was blocked by hardening as viscosity increased with the ex-

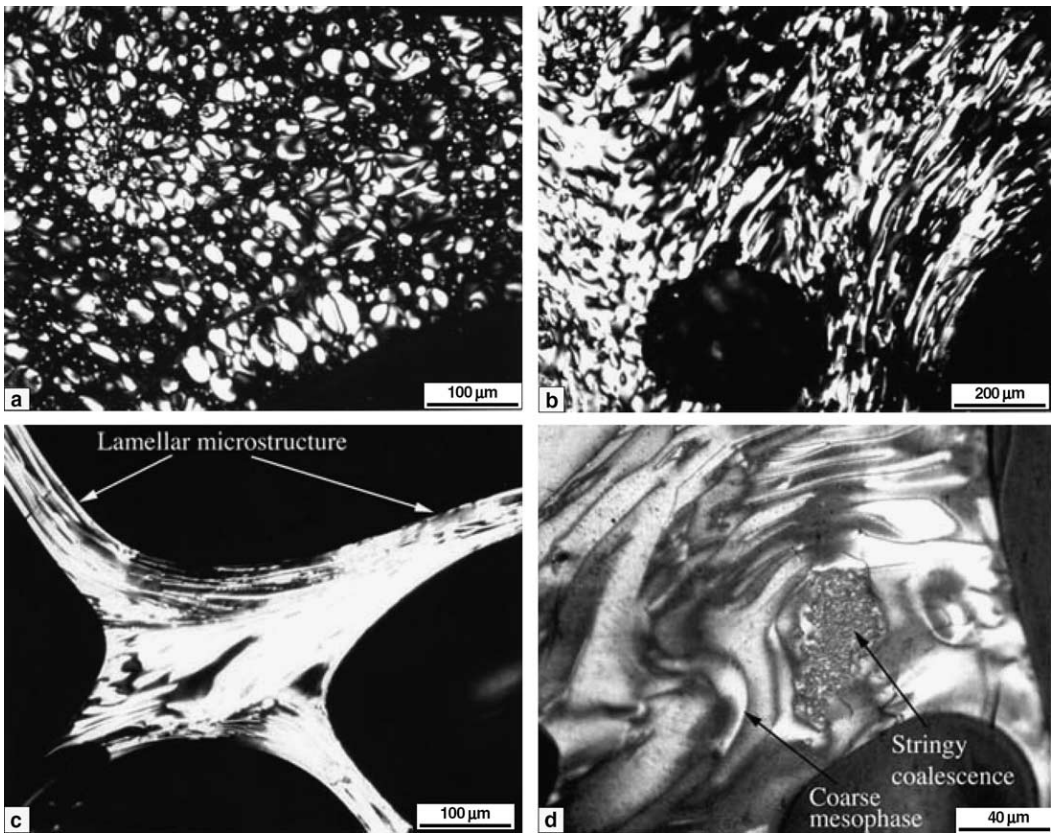

Fig. 1. Polarized-light micrograph of bulk mesophase formation in specimens pyrolyzed to 475 °C at a heating rate of 80 °C/h: (a) spherule formation in quenched sample removed at 350 °C; (b) the formation of microstructures by bubble percolation, 400 °C; (c) higher magnification showing the lamellar microstructure; (d) an island of stringy coalescence captured within coarse microstructure, 475 °C.

tent of mesophase pyrolysis. At this point, the mesophase microstructure was locked in and further heat treatment would lead to formation of shrinkage cracks and sharpening of the folded mesophase layers. With this process, the carbon yield after heat treatment to 475 °C and hold time of 3 h was between 25% and 30%.

In addition to regions of coalesced mesophase consisting of coarse microstructure, a fine isotropic microstructure was evident for the subsequent sample removed at 475 °C (Fig. 1(d)). These microstructures will be referred to as stringy coalescence from here on. Under high-magnification polarized-light microscopy, the fine structure of extinction contours appears as an array of small coalesced spherules having less rearrangement than the coarse microstructure. These fine isotropic structures without long range preferred orientation might result from spherules being in contact with little or no coalescence [15]. Similar structures were observed by White and co-workers [9,10] during pyrolysis of coal-tar and petroleum pitches. They suggested that the stringy coalescence could form if nucleation of spherules occurs more rapidly before their growth and coalescence. Mochida et al. [7] suggested that the fine structure might be due to excess amount of catalyst, which may cause rapid polymerization. More recently Fernandez et al. [16] also observed similar microstructures in unwashed cokes during the pyrolysis of anthracene oil with 10 wt.% $AlCl_3$. Similar to Mochida et al. they suggested that the catalyst in unwashed material causes rapid pyrolysis leading to increased viscosity, which in turn reduces the deformation of the coalesced spherules. Our use of 5 wt.% $AlCl_3$ was based on the works of Fernandez et al. [16] and Mochida et al. [5–7] but our results suggest that lower levels of catalyst addition may be necessary in order to eliminate stringy coalescence.

Bulk mesophase transformation under an applied pressure of 0.7 MPa revealed the same general observation of spherule nucleation, growth, and coalescence during pyrolysis. From the optical observations (see Fig. 3(f)) , it appears that pyrolysis under elevated pressure results in higher yields of mesophase, consisting predominantly of coarse microstructures. However, undesirable stringy coalescence was also found to occur more frequently under high pressure.

3.2. In situ mesophase transformation within preforms

At the early stage of heat treatment, the naphthalene and catalyst mixture constitutes a very low viscosity wetting solution. The viscosity of naphthalene at 100 °C is

0.76 cP [17], much lower than that of pitch-like material. Hence, the mixture can easily and uniformly infiltrate the fiber bundles and the void spaces by capillary forces without applied pressure. The wetting behavior of the melted naphthalene was similar for both the PAN filaments and the ones coated by CVI. As shown in Fig. 2(a), most of the main void spaces were filled with an intermediate isotropic liquid at 325 °C. No mesophase spherules had yet formed at this stage, which was arrived using a heating rate of 80 °C/h and without holding time. As either the temperature or the holding time increased, polymerization of the aromatic mole-

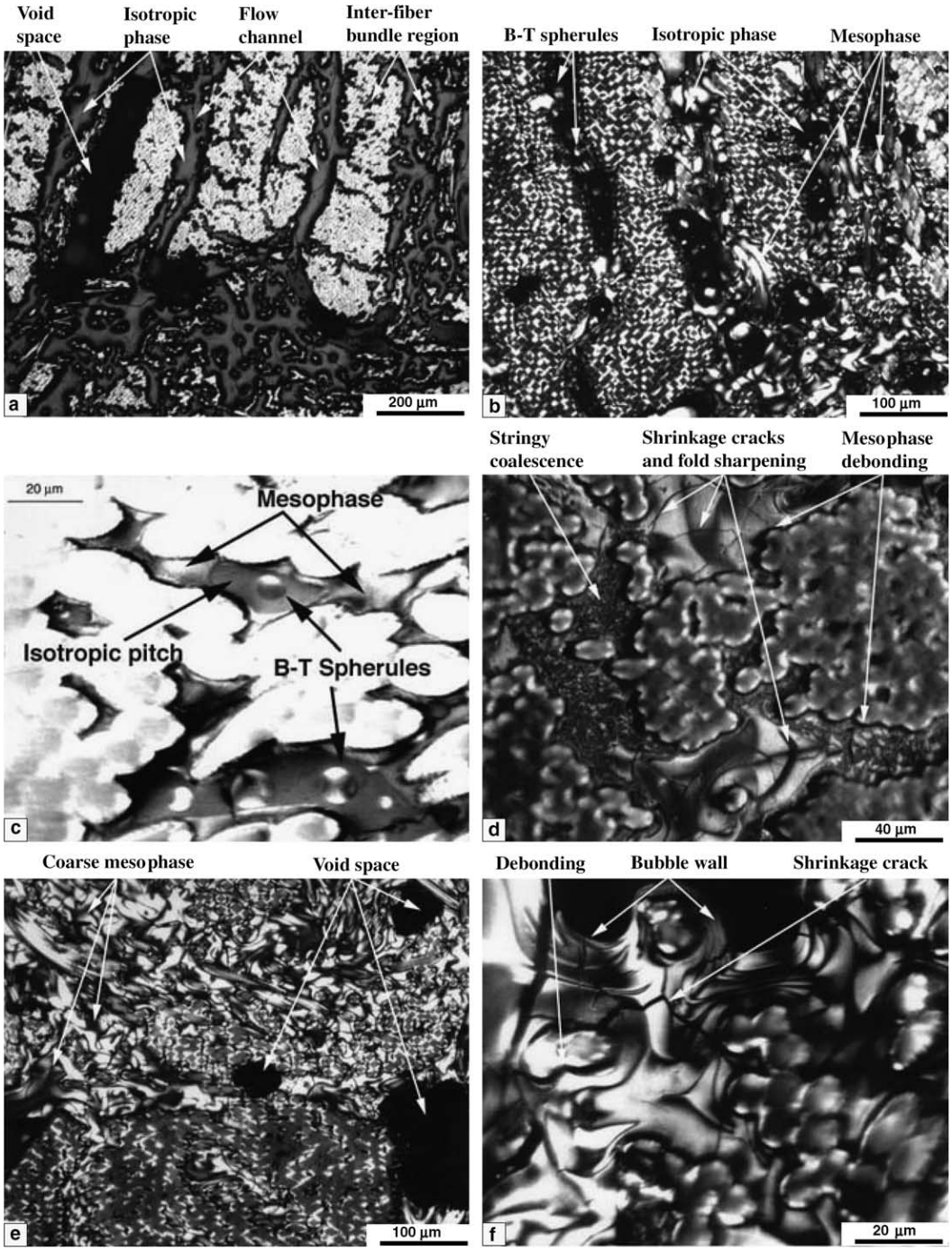

Fig. 2. The mesophase formation within a CVI-rigidized preform cube: (a) an isotropic liquid at 320 °C; (b) B–T spherules observed at 350 °C with zero holding time; (c) formation of B–T spherules in tightly packed fiber bundles; (d) stringy coalescence after 1 h holding at 475 °C; (e) fully transformed structures after 1 h holding at 475 °C; (f) higher magnification view of (e).

cules led to nucleation and growth of mesophase spherules.

The formation and precipitation of mesophase spherules in the flow channels is illustrated with the sample taken at 350 °C in Fig. 2(b), and the presence of mesophase spherules within fiber bundles was evident under higher magnification, as shown in Fig. 2(c). Both isotropic liquid and mesophase pitch wet the CVI-coated filaments. As shown previously [14], the mesophase layers were aligned normal to the isotropic liquid and parallel next to the carbon filament or CVI surface. This image clearly shows that the mesophase transformation within a fiber bundle is similar to those observed in the bulk phase.

As temperature increased to 475 °C, mesophase transformation was mostly complete. After 1 h of holding at 475 °C, most mesophase spherules had coalesced to form coarse carbonaceous mesophase; however, a few regions of stringy structure within fiber bundles were also observed (Fig. 2(d)). Fig. 2(e) provides a low-magnification view of the pyrolyzed preform along a vertical section near the innermost region. The hardened mesophase was mostly retained within the fiber bundles and the regions in between. The major void spaces where nucleation and growth of gas bubbles tend to take place remained unfilled. The high-magnification micrograph (Fig. 2(f)) shows the bloating of the mesophase matrix and the formation of the bubble wall microstructure. The bloating not only led to formation of voids but also forced the matrix into the surrounding regions or expulsed it from the preform. An extensive network of shrinkage cracks was observed within the coarse mesophase matrix upon cooling due to thermal expansion mismatch between the matrix and the filaments.

3.3. Densification of non-rigidized preforms in multiple cycles

3.3.1. Naphthalene and aluminum chloride catalyst

The increase in weight gain and apparent density through five impregnation and carbonization cycles with naphthalene and $AlCl_3$ catalyst is summarized in Table 1. The apparent density of the composite increased with each impregnation cycle, although the incremental change decreased rapidly in cycles three through five. The largest weight gain and incremental density gain were achieved in the first and second cycles, where the molten naphthalene easily penetrates the fiber bundles and the small inter-fiber bundle regions. After two cycles, these regions were well filled with the transformed mesophase. The decrease in incremental weight gain and density change beyond the second cycle can be attributed to less efficient filling of the larger void spaces and the formation of closed pore spaces that prevent penetration of naphthalene. Using the definition of volume efficiency [3], we estimated that the filling efficiencies were approximately 47% and 36%, respectively, during the first two cycles, and afterward, the efficiency fell below 15%. In the efficiency computation, the decrease in porosity after each cycle was calculated from the measured bulk density of the composite after carbonization, the starting void fraction of the non-rigidized preform, and the fiber and the mesophase coke densities. The density value used for the non-rigidized fiber and transformed mesophase heat treated to 1150 °C was 1.73 and 1.90 g/cm^3, respectively. With a significant drop off in the efficiency, the filling of larger void spaces will require multiple cycles in order to reach higher composite densities.

Table 1
Change in weight gain and density in different impregnation cycles with naphthalene-catalyst mixture at ambient pressure

Number of cycles	Percent weight gain[a]		Bulk density[b] (g/cm^3)	Percent incremental density gain
	I	C		
0			0.45	
1	191.1	163.0	1.11	147%
2	26.3	23.7	1.38	24%
3	6.7	5.5	1.45	5.1%
4	3.9	3.3	1.50	3.4%
5	2.4	2.0	1.53	2.0%

[a] Weight gain measured after impregnation, I, and carbonization, C.
[b] Density measured after carbonization to 1150 °C.

Micrographs from the innermost regions of carbonized specimens from the different impregnation cycles are presented in Fig. 3. This set of specimens was pyrolyzed to 475 °C and held at constant temperature for 3 h. Fig. 3(a) clearly indicates that large void space remained after one cycle of impregnation, although the fiber bundles appear to be well filled with mesophase (Fig. 3(b)). The mesophase microstructure in the bundles was determined by the sheath effect such that the alignment of the mesophase layers led to formations of $-\pi$ and -2π disclinations [14]. As compared to the CVI-coated filaments (Fig. 2(f)), there appeared to be good bonding between the filament and the mesophase matrix. The micrographs from the third-cycle impregnation (Fig. 3(c) and (d)) show filling of the shrinkage cracks and most of the inter-fiber bundle regions. There also appears to be a buildup of matrix within the larger void spaces. The image from the fifth cycle (Fig. 3(e)) illustrates the complete filling of the inter-fiber bundle region and the still slow, gradual filling of the larger void space. The preform can further be densified with additional impregnation cycles as long as the void space remains open. At this stage, the effect of matrix bloating, pitch expulsion from the flow channels, and the low carbon yield become increasingly more dominant, as indicated by the small incremental gain in density beyond the third cycle.

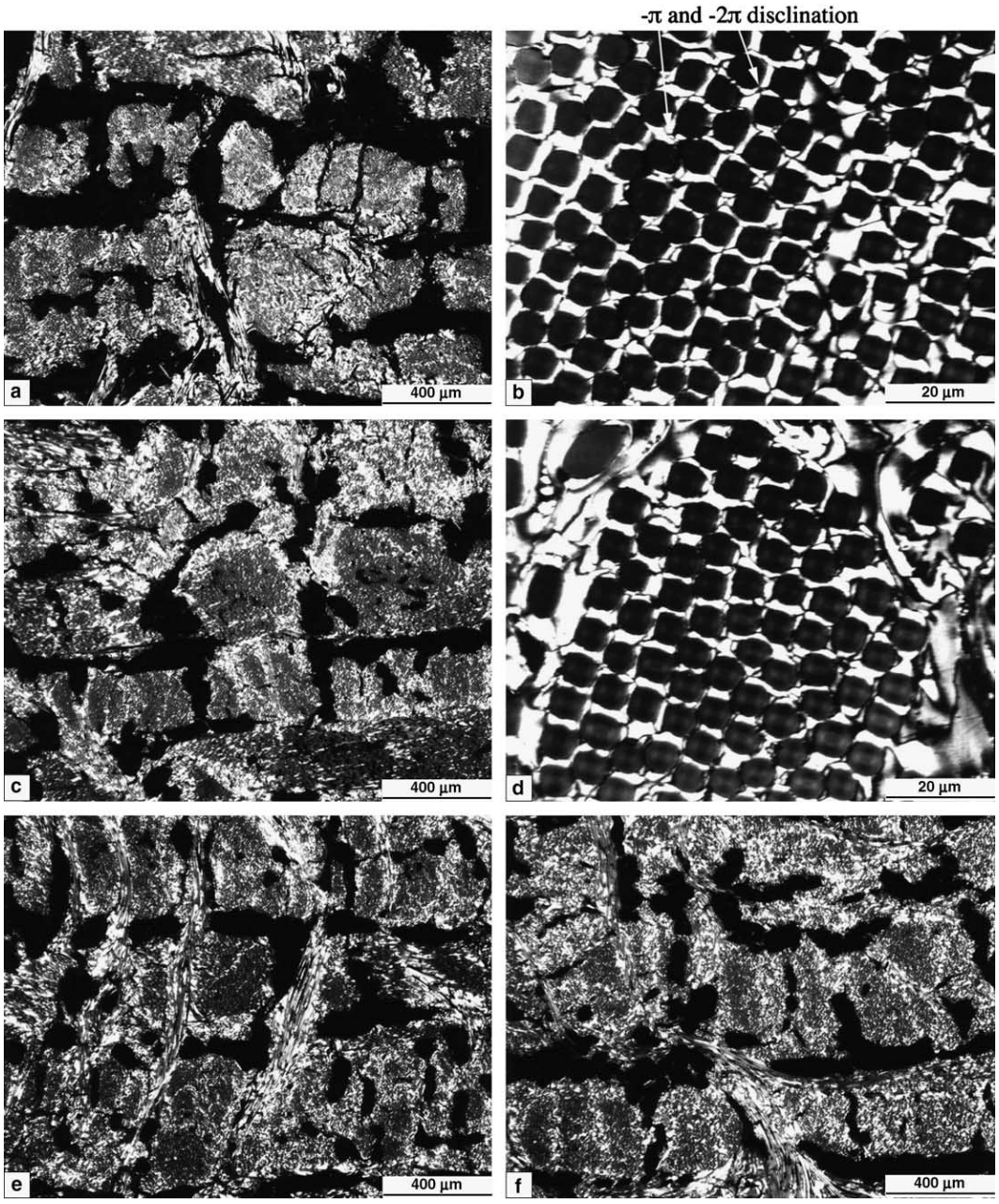

Fig. 3. Mesophase microstructure of the innermost region in specimens pyrolyzed and carbonized at ambient pressure: (a) after the first cycle impregnation; (b) higher magnification view of (a); (c) after the third cycle; (d) higher magnification view of (c); (e) after the fifth cycle; (f) after the third cycle impregnation and transformation under 0.7 MPa.

Applying modest pressures during pyrolysis was observed to improve the densification efficiency. Under 0.7 MPa, the densities of the composite after the first and second cycle were each around 1.2 and 1.47 g/cm^3. These values were approximately 8% higher than those densities attained at room pressure. Fig. 3(f) shows the innermost section of a carbonized specimen after the third-cycle impregnation under pressure. The bulk density of the specimen was measured to be 1.63 g/cm^3, and the filling appears qualitatively to be similar to the impregnation after five cycles at ambient pressure.

3.3.2. AR mesophase pitch

Impregnation with a low-viscosity fully transformed AR mesophase pitch was conducted for comparison without imposed pressure or applied vacuum. The impregnation of non-rigidized preforms was conducted at an upper temperature limit of 350 °C in order to avoid thermal degradation of the AR mesophase pitch [18]. The viscosity of AR mesophase at 350 °C is about 10^4 cP [19,20], several orders of magnitude greater than that of naphthalene. As a result, the pitch cannot penetrate uniformly larger samples under ambient pressure.

Table 2
Change in weight gain and density in different impregnation cycles with AR mesophase pitch at ambient pressure

Number of cycles	Percent weight gain[a]		Bulk density[b] (g/cm^3)	Percent incremental density gain
	I	C		
0			0.42	
1	213	181	1.19	183%
2	28.8	23.6	1.47	24%
3	9.5	7.6	1.58	7.5%

[a] Weight gain measured after impregnation, I, and carbonization, C.
[b] Density measured after carbonization to 1150 °C.

Hence, all impregnation runs using AR pitch necessarily required the use of the smaller 8 mm-sized preforms.

Weight gain and density measurements after each impregnation cycle are summarized in Table 2. The density of the composite rose to 1.47 g/cm^3 after two cycles, as compared with three cycles in Table 1. The key difference appears to be the slightly higher incremental density gain achieved during the first cycle. The density gain dropped back to 24% in the second cycle. In terms of filling efficiency, we estimated that it was about 49% during the first cycle, and lowered to 36% during the second cycle. Even at the third cycle, the incremental density gain was 7.5%, and the filling efficiency was approximately 22%. The composite achieved a density of 1.58 g/cm^3 after the third cycle.

While these figures appear much more attractive than using naphthalene in situ transformation, one needs to recognize the much higher viscosity of the AR mesophase. In-depth penetration of mesophase impregnation under ambient pressure is limited in scale [21], and as in this work, to very small preform samples. Under more practical situations, one would use pressure injection or apply a vacuum. One may consider raising the impregnation temperature above the present 350 °C. However, higher temperatures will approach the thermal stability of the AR mesophase leading to formation of bubbles and increased viscosity [18].

The inner and outer regions of stabilized and carbonized specimens after the first cycle are shown in Fig. 4(a) and (b), respectively. Low-temperature oxidation stabilization [11] was effective in retaining the impregnated mesophase during the carbonization with carbon yields of about 90%. As a result, higher densities were achieved in AR impregnated preforms than the preforms densified by in situ transformation process. However, as

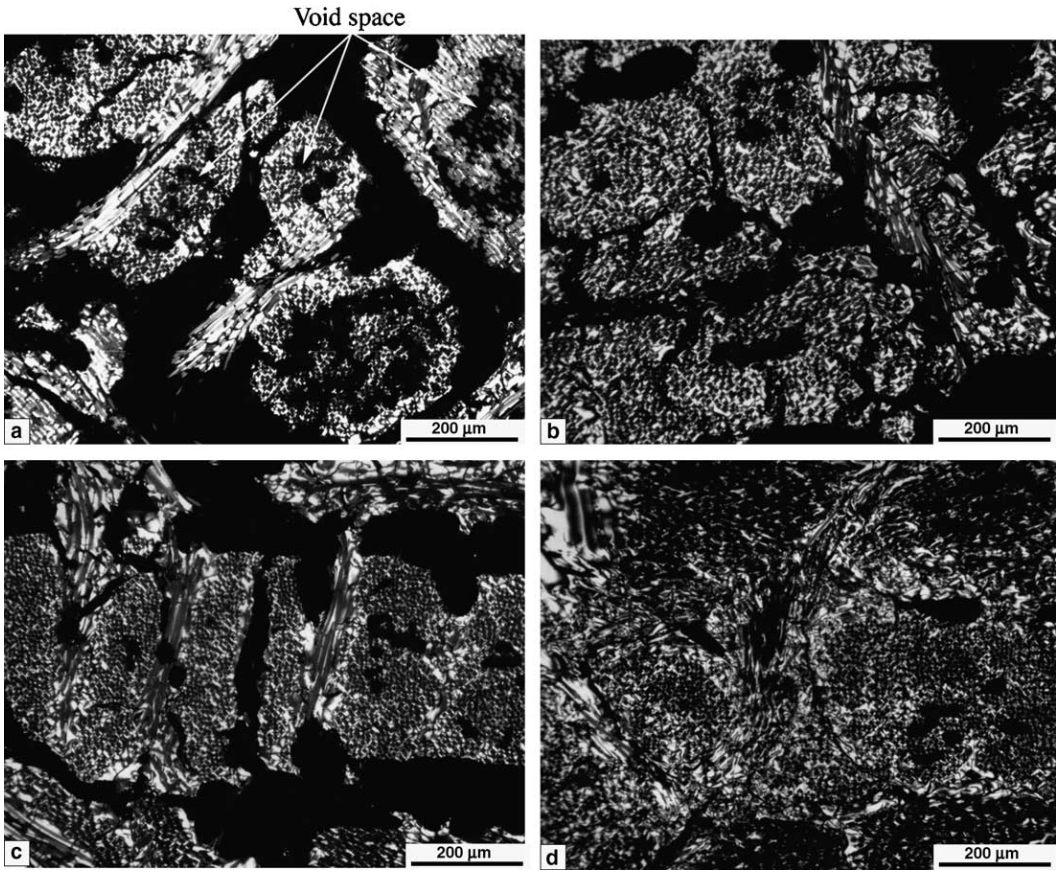

Fig. 4. Microstructure of stabilized and carbonized specimens impregnated with AR mesophase: (a) after the first cycle, inner region; (b) first-cycle, outer region; (c) third-cycle, inner region; (d) third-cycle, outer region.

shown in Fig. 4, the extent of mesophase penetration decreases from the outer edge to the center of the preform, resulting in non-uniform filling. In Fig. 4(a), the inter-fiber bundle regions and the large void spaces remain largely unfilled. With an additional impregnation cycle the pathways for penetration of mesophase to the inner regions become filled. After the third-cycle impregnation the void spaces in inner region remain unfilled, whereas they are mostly filled in the outer region (Fig. 4(c) and (d)). Significant blockage of access channels at the outer edge will significantly limit the access of mesophase to the innermost regions in the subsequent impregnation cycles.

4. Conclusions

The mesophase microstructures formed in bulk specimens during the pyrolysis of naphthalene mixed with $AlCl_3$ catalyst include the three main microconstituents observed in needle cokes; coarse, fibrous, and lamellar. The naphthalene catalyst mixture easily penetrates the carbon preform at ambient pressure and the mesophase transformation process within the large void spaces and fiber bundles are similar to the observation in the bulk specimens. The impregnation is efficient in filling tightly packed fiber bundles but not large open channels. Multiple impregnation cycles are required in order to fill the large void spaces.

With consideration of the different merits of in situ transformation and mesophase injection, it may be fruitful to explore an integrative approach that utilizes both processes at different cycles. For example, an initial impregnation cycle can be applied as a low-cost alternative to CVI-rigidization. This is followed by a small number of injection cycles. Toward higher density ranges, impregnation can be applied as a final densification step.

Acknowledgements

We thank Michael Mauldin for experimental assistance, J. Zimmer for helpful discussions, and the Mitsubishi Gas-Chemical Company for provision of AR mesophase pitch.

References

[1] Fathollahi B, Chau PC, White JL. Injection and stabilization of mesophase pitch in the fabrication of carbon–carbon composites: Part I. Injection process. Carbon 2005;43:125–33.

[2] White JL, Sheaffer PM. Pitch-based processing of carbon–carbon composites. Carbon 1989;27:697–707.

[3] Matzinos PD, Patrick JW, Walker A. The efficiency and mechanism of densification of 2-D C/C composites by coal-tar impregnation. Carbon 2000;38:1123–8.

[4] Wapner PG, Hoffman WP, Jones B. Carbon and ceramic matrix composites fabricated by a rapid low-cost process incorporating in situ polymerization of wetting monomers. US Patent 6,309,703 B1; 2001.

[5] Mochida I, Nakamura E, Maeda K, Takeshita K. Carbonization of aromatic hydrocarbons—III: carbonization catalyzed by alkali metals. Carbon 1975;13:489–93.

[6] Mochida I, Nakamura E, Maeda K, Takeshita K. Carbonization of aromatic hydrocarbons—IV: Reaction path of carbonization catalyzed by alkali metals. Carbon 1976;14:123–9.

[7] Mochida I, Inoue S, Maeda K, Takeshita K. Carbonization of aromatic hydrocarbons—VI: Carbonization of heterocyclic compounds catalyzed by aluminum chloride. Carbon 1977;15:9–16.

[8] Mochida I, Shimizu K, Korai Y, Sakai Y, Fujiyama S, Toshima H, et al. Mesophase pitch catalytically prepared with HF/BF_3 from anthracene. Carbon 1992;30:55–61.

[9] Dubois J, Agache C, White JL. The carbonaceous mesophase formed in the pyrolysis of graphitizable organic materials. Metallography 1970;3:337–69.

[10] White JL, Price RJ. The formation of mesophase microstructures during the pyrolysis of selected coker feedstocks. Carbon 1974;12:321–33.

[11] Fathollahi B, Jones B, Chau PC, White JL. Injection and stabilization of mesophase pitch in the fabrication of carbon–carbon composites. Part III: Mesophase stabilization at low temperatures and elevated oxidation pressures. Carbon 2005;43:143–51.

[12] Rey Boero JF, Wargon JA. Study of the $AlCl_3$ catalytic on aromatic hydrocarbons II: Mesophase formation. Extended Abstracts Carbon'79 (University Park, PA) 1979:342–3.

[13] Lewis IC. Thermal polymerization of aromatic hydrocarbons. Extended Abstracts Carbon'79 (University Park, PA) 1979:397–8.

[14] Zimmer JE, White JL. Disclination structures in the carbonaceous mesophase. Adv Liquid Cryst 1982;5:157–213.

[15] Zimmer JE. Proper description of mesophase microstructures. Extended Abstracts Carbon'91 (Santa Barbara, CA) 1991:154–5.

[16] Fernandez AL, Granda M, Bermejo J, Menendez R. Catalytic polymerization of anthracene oil with aluminium trichloride. Carbon 1999;37:1247–55.

[17] Grzyll LR, Ramos C, Back DD. Density, viscosity, and surface tension of liquid quinoline, naphthalene, biphenyl, decafluorobiphenyl, and 1,2-diphenylbenzene from 300 to 400 °C. J Chem Eng Data 1996;41:446–50.

[18] White JL, Gopalakrishnan MK, Fathollahi B. A processing window for injection of mesophase pitch into a fiber preform. Carbon 1994;32:301–10.

[19] Khandare PM, Zondlo JW, Stansberry PB, Stiller AH. Rheological investigation of pitch material. Part II: Viscosity measurement of a240 and ara-24 pitches using a high-temperature high-pressure rheometer. Carbon 2000:889–97.

[20] Dumont M, Dourges MA, Pailler R, Bourrat X. Mesophase pitches for 3d-carbon fibre preform densification: rheology and processability. Fuel 2003;82:1523–9.

[21] Dumont M, Pailler R, Bourrat X. Mesophase-pitch for low pressure carbon/carbon composite processing. Extended Abstracts Carbon'04 (Providence, RI) 2004.

APPENDIX D

"Integrated Mesophase Injection and In-Situ Transformation in Fabrication of High Density Carbon-Carbon Composites"

B. Fathollahi, M. Mauldin, P. C. Chau, P. G. Wapner, and W. P. Hoffman

Carbon, 44, 854 (2006)

Available online at www.sciencedirect.com
SCIENCE DIRECT
Carbon 44 (2006) 854–858
CARBON
www.elsevier.com/locate/carbon

Integrated mesophase injection and in situ transformation in fabrication of high-density carbon–carbon composites

B. Fathollahi [a,*], M. Mauldin [a], P.C. Chau [a], P.G. Wapner [b], W.P. Hoffman [c]

[a] Chemical Engineering Program, University of California, San Diego, La Jolla, CA 92093-0411, USA
[b] ERC Inc., 10 East Saturn Blvd., Edwards, CA 93524, USA
[c] Air Force Research Laboratory, 10 East Saturn Blvd., Edwards, CA 93524, USA

Received 15 August 2005; accepted 17 October 2005
Available online 29 November 2005

Abstract

The fabrication of high-density carbon–carbon composite by integrating mesophase injection and in situ transformation methods in different processing cycles was examined. Non-rigidized preform disks 30 mm thick and 68 mm in diameter were rigidized by an initial in situ transformation cycle to an average density of 0.92 g/cm^3 after carbonization. The rigidized preforms were subsequently densified by 1–3 cycles of injection with the AR mesophase pitch. After each injection cycle, the flow-oriented mesophase matrix was stabilized and carbonized to 1150 °C. The composites from each injection cycle were further densified by a final in situ cycle. A final density of nearly 2 g/cm^3 was attained after three injection cycles and a final in situ cycle. All the cycles except the third injection required only ambient or very moderate pressures.

Keywords: Carbon composite; Mesophase; Microstructure; Optical microscopy

1. Introduction

Several approaches to the fabrication of carbon–carbon (C/C) composites by the pitch-based processes that seek benefits of high-carbon yield, low cost, and good graphitizability have been reported in the past [1–5]. Recently, we have reported two alternative approaches to the fabrication of mesophase-based C/C composites. In one, a rigidized preform is *injected* with a fully transformed mesophase pitch. The oriented mesophase matrix is further stabilized by low-temperature oxidation in order to retain the flow-induced microstructure and to increase carbon yield upon carbonization [6–9]. A second approach is to *impregnate* the preform with a pure wetting monomer (for example, naphthalene) mixed with a catalyst followed by in situ mesophase transformation at ambient or moderate pressures [10,11]. For brevity, these two approaches will be referred to as the injection and in situ methods.

These two methods have their own advantages and disadvantages. The in situ process involves relatively quick and inexpensive processing cycles. The method fills fiber bundles in the initial cycle effectively where the microstructure is dominated by sheath effect [12], but it is inefficient in filling large void regions and thus requires five or more impregnation cycles to reach a density of 1.5 g/cm^3 and higher [10]. Mesophase injection, on the other hand, can fill large void spaces effectively, and with proper stabilization, is capable of retaining flow-induced microstructures, attaining carbon yields of nearly 90% after carbonization, and raising the density to above 1.7 g/cm^3 within a few cycles [7]. However, to prevent compaction, the injection method is best applied to a rigidized preform that often is prepared by slow CVI processes. Because of the high-mesophase viscosity, additional cycles beyond the second would require higher pressures and longer injection times with diminishing returns in density gain.

* Corresponding author. Tel.: +1 858 395 8653; fax: +1 858 534 4543.
E-mail address: bfatholl@ucsd.edu (B. Fathollahi).

0008-6223/$ - see front matter © 2005 Elsevier Ltd. All rights reserved.
doi:10.1016/j.carbon.2005.10.030

Our previous results [7,8,10] point toward a possibly more effective fabrication of high-density C/C composites by integrating the injection and in situ methods. The key is to replace the initial CVI rigidization by an in situ step that applies a "light" impregnation, in the sense of lower filling efficiency, leaving the major flow channels open. Injection cycles are then used to effect densification quickly and emplace a flow-induced orientation. A final in situ cycle is applied to fill any remaining pore space, especially when injection conditions may become increasingly severe. In this short report, we have made density measurements and polarized-light micrograph observations to study the effectiveness of densification of non-woven preforms by integrating the in situ and injection approaches.

2. Experimental methods

As-received non-woven preforms cut from brake disks, 30 mm in thickness and 68 mm in diameter, having a volume fraction of 26% and a density of 0.45 g/cm^3 were used. Details of the preform architecture and experimental procedures of in situ impregnation and mesophase injection, stabilization and carbonization all followed previous works [7,8,10]. All the preforms were first rigidized with an in situ cycle in a pyrolysis chamber by impregnation with naphthalene mixed with 5 wt.% $AlCl_3$ as the catalyst. A flow of nitrogen is maintained above the closed chamber during pyrolysis of the impregnated naphthalene. The average bulk density of the rigidized preform after heat treatment to 1150 °C was 0.92 g/cm^3.

The rigidized preforms were subsequently densified by 1–3 cycles of injection with the ARA24R mesophase pitch having a softening point of 297 °C and a density of 1.3 g/cm^3. After each injection cycle, the mesophase matrix was stabilized at 170 °C and carbonized to 1150 °C. The carbonized sample from each of the injection and stabilization cycles was further densified by a final in situ cycle. Bulk density was calculated from the weight and volume of a disk sample. The density of the carbonized composite after the final in situ cycle was measured by helium picnometer. The volumetric filling efficiency was estimated from the ratio of the carbonized mesophase coke volume to the void volume before each cycle [6]. In the computation of the efficiency, the density of the non-rigidized PAN fiber was taken as 1.73 g/cm^3, the density of the mesophase matrix heat-treated to 1150 °C was 2.05 g/cm^3 for ARA24R [13] and 1.9 g/cm^3 when starting with naphthalene. The microstructure of the carbonized specimens after each cycle was examined by reflected polarized-light microscopy.

3. Results and discussion

The processing conditions, density measurements, and the estimated filling efficiency of each cycle are summarized in Table 1. All three specimens (A-1, B-1, and C-1) underwent an initial in situ rigidization and the first injection cycle. As shown in Fig. 1a, which represents the specimens after the initial in situ rigidization but prior to the first injection, large interconnected void spaces among fiber bundles remained unfilled and are accessible to mesophase

Table 1
Summary of process conditions and results after multiple injection cycles

Injection cycles	First			Second	Second	Third
Specimen	A-1	B-1	C-1	B-2	C-2	C-3
Initial density (g/cm^3)	0.926[a]	0.915[a]	0.926[a]	1.43	1.44	1.75
Filling efficiency, estimate (%)	33.9	33.1	33.9			
Injection conditions						
Temperature (°C)	304	304	304	325	325	350
Pressure (MPa)	0.63	0.64	1.1	0.7	2.2	2.4
Time under pressure (h)	1.22	1.25	0.58	2.01	0.16	0.53
Mesophase throughput[b] (g)	30	15	20	15	15	0
After injection						
Mesophase mass-fraction	0.39	0.4	0.39	0.17	0.19	0.077
ρ (g/cm^3)	1.53	1.52	1.52	1.75	1.79	1.89
$\Delta\rho$ (g/cm^3)	0.604	0.605	0.594	0.29	0.34	0.14
After carbonization						
ρ (g/cm^3)	1.44	1.43	1.44	1.67	1.75	1.88
Filling efficiency, estimate (%)	51.1	50.4	51.2	41.2	57.3	60.8
Final in situ cycle and carbonization						
ρ (g/cm^3)	1.61			1.80		1.97
$\Delta\rho$ (g/cm^3)	0.17			0.13		0.09
Filling efficiency, estimate (%)	38.1			35.0		–[c]

Samples A-1, B-2, and C-3 are further treated with an additional in situ cycle.
[a] Density after initial in situ impregnation and carbonization.
[b] Mass of mesophase collected at the pitch exit of injection device.
[c] Not available. See text for discussion.

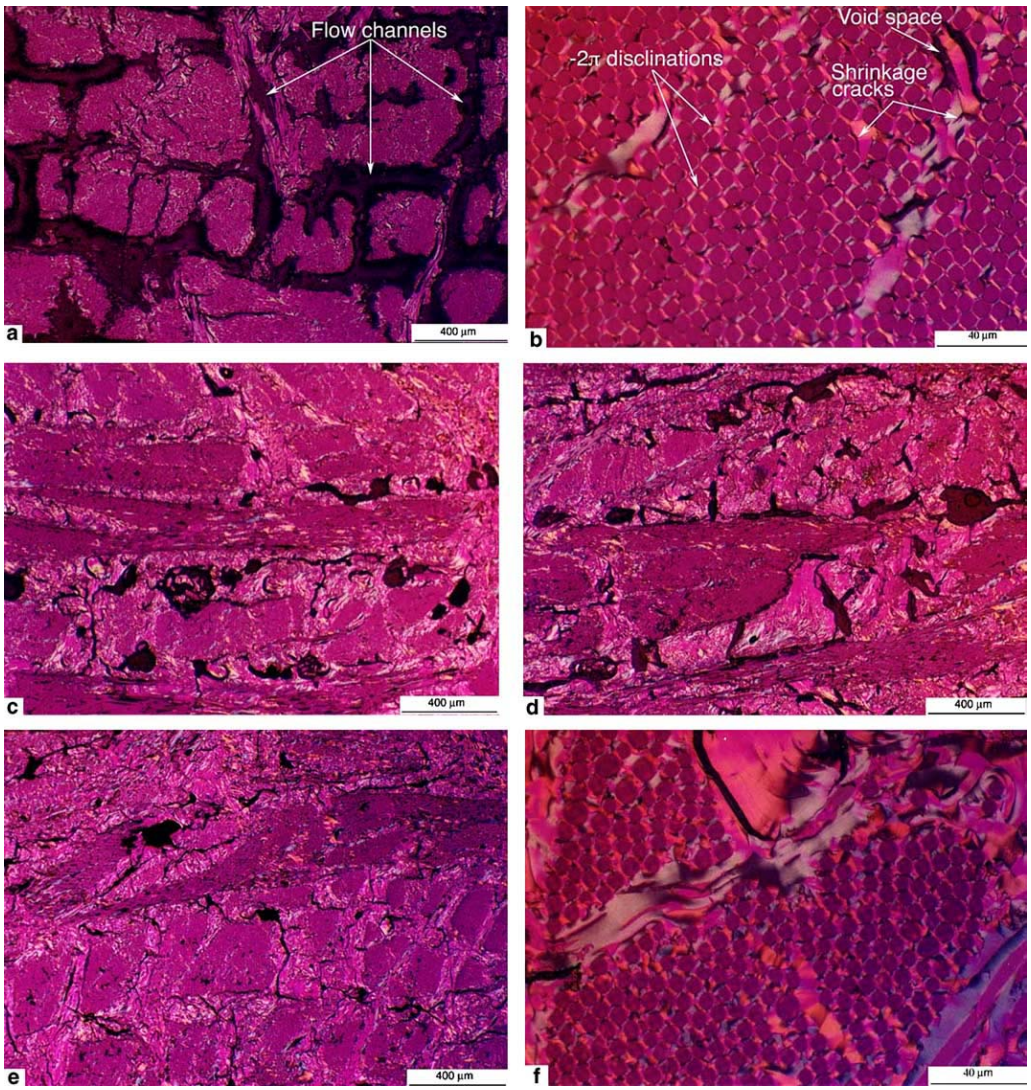

Fig. 1. Longitudinal section of carbonized composites: (a, b) low- and high-magnification views after the initial in situ cycle; (c) A-1 with 1 injection and final in situ cycles; (d) B-2 with 2 injections and final in situ; (e ,f) low and high magnification of C-3 with 3 injections and a final in situ cycle.

injection. The high-magnification micrograph (Fig. 1b) shows that the fiber bundles are relatively well filled with mesophase layers aligned parallel to the filaments, and with visible -2π disclinations. Nonetheless, there are still void spaces within the inter-fiber bundle region and shrinkage cracks that remain to be filled in subsequent cycles.

During the first injection cycle, two different pressures were used, 0.64 MPa on specimen B-1 and a higher 1.1 MPa on C-1. The injection time for C-1 was cut in half by nearly doubling the injection pressure and without compromising the density achieved. The oxygen mass gain of the mesophase matrix for the three specimens was approximately 10% resulting in carbonization yields of about 86%. The estimated filling efficiency averaged about 51% for the first-cycle injection. The filling efficiency using the in situ method alone was only about 36% in the second cycle, and the density was 1.38 g/cm^3 after carbonization [10]. It took a third in situ cycle to reach a density of 1.45 g/cm^3. The first cycle by in situ method alone is equivalent to the preform rigidization step described here.

In the present approach, the density after carbonization reached on average 1.44 g/cm^3 after one injection cycle, or the second processing cycle counting the initial rigidization. The density of A-1 was further raised to 1.6 g/cm^3 after the additional in situ cycle. If only the in situ method had been used [10], five cycles at ambient pressure would have been needed to attain this density level. While the filling efficiency of the in situ method can be improved by applying modest pressures during pyrolysis, this was not attempted here because the focus is on the feasibility of integrating the injection and in situ methods.

Furthermore, we should point out the probable trade off in the extent of transformation during the initial in situ cycle. We have carried out longer in situ cycles on several preforms during the initial rigidization and raised the density to 1.1 g/cm^3 or higher. However, after one injection

cycle with these samples, the filing efficiencies were under 36%, and the highest density attained was only 1.39 g/cm^3. These results suggest that the flow channels might have become more restricted or not as easily accessible to flowing mesophase. Thus, even though one could raise the density beyond 0.9 g/cm^3 during rigidization, it may not be beneficial because of the substantial decrease in filling efficiencies in subsequent injection cycles. It would be more advantageous to perform a shorter in situ step to achieve just adequate rigidization to permit more open flow channels for injection.

A second injection cycle was applied to specimens B-1 and C-1, which became B-2 and C-2. Again, two different injection pressures were used. The trade off becomes more distinct here. With only a moderate pressure of 0.7 MPa on specimen B-2, the injection took about 2 h. The injection time was reduced drastically to 0.16 h if one finds it affordable to raise the pressure to 2.2 MPa. The difference may also point to the filling of most accessible flow channels during the first injection cycle. Under a higher injection pressure, the bulk density was marginally greater for C-2 (1.75 vs. 1.67 g/cm^3 for B-2) but the filling efficiency was 16% higher, which may suggest that the increase in pressure was more effective in filling small void spaces. The density of B-2 was further raised to 1.8 g/cm^3 after applying an additional in situ cycle. It is noteworthy that such a density has been achieved under very moderate injection conditions (0.7 MPa for B-2) and a total of four processing cycles including the initial and final in situ steps.

The micrographs of A-1 and B-2, after one and two injections with the final in situ cycle are shown in Fig. 1c and d, respectively. Under low magnification, these images do not appear too differently, possibly because their densities differ by a slight 0.19 g/cm^3. In both specimens, the fiber bundles and inter-fiber bundle region appear to be well filled with mesophase layers aligned parallel to filament surfaces. Flow-induced microstructure was retained in the main flow channels. However, there are still void spaces and shrinkage cracks created by thermal densification of mesophase matrix that remain to be filled.

A third injection cycle was applied to specimen C-2, which became C-3. Compared with the processing of B-2, much more severe injection conditions are now required. Even with the injection pressure raised to 2.4 MPa and a temperature approaching the stability of the mesophase pitch, no mesophase throughput was observed. The filling efficiency under the high-pressure injection was about 60%; however, the density of 1.88 g/cm^3 was only slightly higher then the final density of B-2 after a much easier in situ step. It is evident that most of the major flow channels are well filled after the second injection cycle and it may be more economical to begin switching over to in situ methods for further densification. A final in situ cycle was applied to C-3 to achieve a density of 1.97 g/cm^3. The filling efficiency of this final cycle is omitted in Table 1. The very small remaining void volume leads to a cumulative estimation error that is large enough that we do not believe the quantity would be reliable.

The micrograph of C-3 in Fig. 1e confirms that the flow channels are now well filled throughout the composite. In comparison to Fig. 1d, it is also evident that a high-pressure injection is needed to fill any remaining open channels. The high-magnification image (Fig. 1f) of the fiber bundles shows complete filling of inter-fiber bundle regions, with less minute unfilled gaps that are evident still in Fig. 1b. There remains still some small unfilled space. They may represent closed void spaces that are no longer accessible by either injection or in situ methods.

4. Conclusion

A carbon–carbon composite consisting of a mesophase matrix with a final density of nearly 2 g/cm^3 has been attained relatively easily with a total of five processing cycles that included an initial rigidization step. Except for the third injection, all other cycles, including the first two injections, required only ambient or very moderate pressures. This work point toward the feasibility of sandwiching injection cycles between in situ steps for rigidization and final filling of minute void spaces.

Acknowledgements

We thank J. Zimmer for helpful discussions, G. Cole for experimental assistance, and the Mitsubishi Gas-Chemical Company for provision of AR mesophase pitch.

References

[1] White JL, Sheaffer PM. Pitch-based processing of carbon–carbon composites. Carbon 1989;27:697–707.
[2] Christ K, Huttinger KJ. Carbon–carbon-reinforced carbon composites fabricated with mesophase pitch. Carbon 1993;31:731–50.
[3] Granda M, Patrick JW, Walker A, Casal E, Bermejo J, Menendez R. Densification of unidirectional C/C composites by melted pitch impregnation. Carbon 1998;36:943–52.
[4] Matzinos PD, Patrick JW, Walker A. The efficiency and mechanism of densification of 2-D C/C composites by coal-tar impregnation. Carbon 2000;38:1123–8.
[5] Dumont M, Pailler R, Bourrat X. Mesophase-pitch for low pressure carbon/carbon composite processing. Extended Abstracts Carbon'04, Providence, RI; 2004.
[6] White JL, Gopalakrishnan MK, Fathollahi B. A processing window for injection of mesophase pitch into a fiber preform. Carbon 1994;32:301–10.
[7] Fathollahi B, Chau PC, White JL. Injection and stabilization of mesophase pitch in the fabrication of carbon–carbon composites: Part I. Injection process. Carbon 2005;43:125–33.
[8] Fathollahi B, Chau PC, White JL. Injection and stabilization of mesophase pitch in the fabrication of carbon–carbon composites: Part II. Stabilization process. Carbon 2005;43:135–41.
[9] Fathollahi B, Jones B, Chau PC, White JL. Injection and stabilization of mesophase pitch in the fabrication of carbon–carbon composites: Part III: Mesophase stabilization at low temperatures and elevated oxidation pressures. Carbon 2005;43:143–51.
[10] Chioujones KM, Ho W, Fathollahi B, Chau PC, Wapner PG, Hoffman WP. Microstructural analysis of in situ mesophase

transformation in the fabrication of carbon–carbon composites. Carbon 2006;44:284–92.
[11] Fernandez AL, Granda M, Bermejo J, Menendez R. Catalytic polymerization of anthracene oil with aluminium trichloride. Carbon 1999;37:1247–55.
[12] Zimmer JE, White JL. Disclination structures in the carbonaceous mesophase. Adv Liquid Cryst 1982;5:157–213.
[13] Fujiura R, Watanabe F, Shigematsu R, Kanno K, Kojima T, Komasu M, et al. Recent applications of the synthetic mesophase pitch (AR pitch) catalytically produced from aromatic hydrocarbons with a super acid of HF/BF_3. Extended Abstracts (pdf file 158) Carbon'03, Oviedo, Spain; 2003.

APPENDIX E

"Carbonization Studies of Glassy Carbon Derived From Bis-ortho-Diynylarenes (BODA),"

S.T Iacono, M.W. Perpall, W.P. Hoffman, P.G. Wapner, and D.W. Smith,
Poly. Prep., 47, 75 (2006)

This Page Intentionally Left Blank

CARBONIZATION STUDIES OF GLASSY CARBON DERIVED FROM BIS-*ORTHO*-DIYNYLARENES (BODA)

Scott T. Iacono[1], Mark W. Perpall[1], Wesley P. Hoffman[2], Phillip G. Wapner[3], and Dennis W. Smith, Jr.[*,1]*

[1]Department of Chemistry, Advanced Materials Research Laboratories, Clemson University, Clemson, SC 29634

[2]Air Force Research Laboratory, Propulsion Directorate 10 East Saturn Blvd, Edwards Air Force Base, CA 93524

[3] ERC Inc., 10 East Saturn Blvd, Edwards Air Force Base, CA 93524

*corresponding author e-mail: dwsmith@clemson.edu

Introduction

We have demonstrated bis-*ortho*-diynylarene (BODA) monomers undergo Bergman cyclopolymerizations to form hyper-branched, rigid naphthalene networks that can be further carbonized at 1000 ºC to form glassy carbon in high yield (>80 %) (**Figure 1**).[1] It was shown by Bergman that 1,2-aromatic diacetylenes undergo concerted thermal annulations via a 1,4-diradical intermediate to form functionalized aromatic systems.[2] Tour has further demonstrated enediynes can undergo thermally induced cyclopolymerizations forming linear and branched poly(phenylenes).[3] Such linear polyarylenes have been shown to be inherently difficult to process into carbon-based structures due to their low molecular weight and insolubility. On the other hand, glassy carbon materials are ideal for microstructure fabrication because good thermal stability, electrical conductivity, gas impermeability, and low coefficient of thermal expansion.[4] More so, BODA-derived glassy carbon has shown utility as thin film dielectrics,[1] photonic materials,[5] precursors for carbon fibers,[6] and microstructures formed by micromolding in capillaries (MIMIC).[7] The unique ability to melt or solution process the cured intermediate as shown in **Figure 1** is a key feature to producing such materials. The spacer (X) and terminus (R) can be functionalized in order to tune the range of processing temperatures and wetting capabilities. In our ongoing effort to fabricate carbon-based microstructures[9] via MIMICs, BODA-derived glassy carbon demonstrates excellent shape retention and high carbon yield for the production of near net-shaped components.

Cure cycles of BODA-derived intermediates have been previously investigated using a differential scanning calorimeter (DSC).[10] However, studies on high temperature heat treatments (HTTs) to form glassy carbon are the focus of this investigation. Herein, we show the coefficient of thermal expansion (CTE) studies of several BODA-derived glassy carbon and study their carbonization cycles.

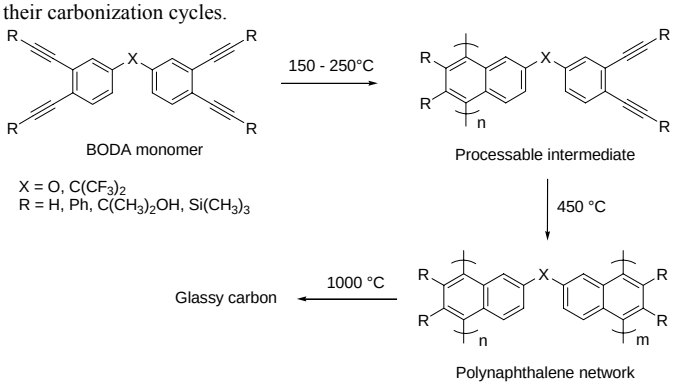

Figure 1. Thermal Bergman cyclopolymerization of bis-*ortho*-diynlarene (BODA) monomers.

Experimental

Materials. Synthesis and characterization of BODA monomers **1–3** (**Figure 2**) were reported elsewhere.[1] Monomer **4** was donated by Dow Chemical. Co-monomers were prepared by mixing with a mortar and pestle a 1:4 weight ratio of **2** and **3** (denoted co-monomer **A**) as well as **2** and **4** (denoted co-monomer **B**).

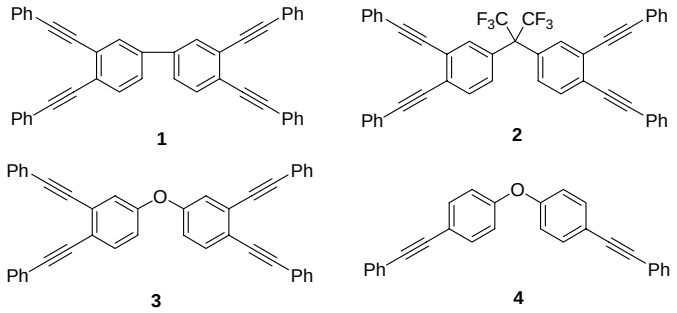

Figure 2. BODA monomers as precursors for high yield glassy carbon.

Instrumentation. A vertical Linseis dilatometer L75 with single push rod was study carbonization and measure CTE. STM measurements were performed by a Digital Instruments Nanoscope III. X-ray powder diffraction was performed using a Scintag XDS 2000 with a voltage of 24 kV.

Sample Preparation. Sample dilatometer discs were prepared by placing monomer or co-monomer powder (ca. 100 mg) in machined single bore extrusion mullite molds (Vesuvius McDaniel, 6.35 mm O.D. and 4.75 mm I.D.). The monomer or co-monomer was then heated in a Lindbergh furnace from ambient temperature to 350 ºC at a ramp of 10 ºC/min under a constant flow of nitrogen. The samples were then further cured at 350 ºC for 48 hours. The solid disks were removed by machining away the mullite mold and were used without further cleaning. The prepared cured solid disks tested for CTE had a nominal diameter and thickness of 6.35 mm in 2.34 mm, respectively.

Cured sample disks were then heated in argon from ambient to 1000 ºC or 1500 ºC at 10 ºC/min. The carbonized samples were cooled to room temperature under argon. Carbonized samples were then reheated from ambient to 1000 ºC or 1500 ºC at 10 ºC/min to determine their CTE. The CTE (α) was determined by linear graphical regression using the equation $\alpha = (1/L_0)(\Delta L/\Delta T)$, where L_0 is the initial sample length, ΔL is the change in length from ambient to elevated temperature, and ΔT is the change in temperature from ambient. Measurements were taken in triplicate for each sample.

Results and Discussion

Co-monomers **A** and **B** were the focus of this investigation because they demonstrate accelerated cure times at lower temperatures compared with monomer precursors **1–3**.[9] A representative carbonization cycle of cured BODA co-monomer **A** is shown in **Figure 3**. It shows the onset of carbonization temperature (T_{onset}), as determined graphically by the initial dimensional change in sample length.

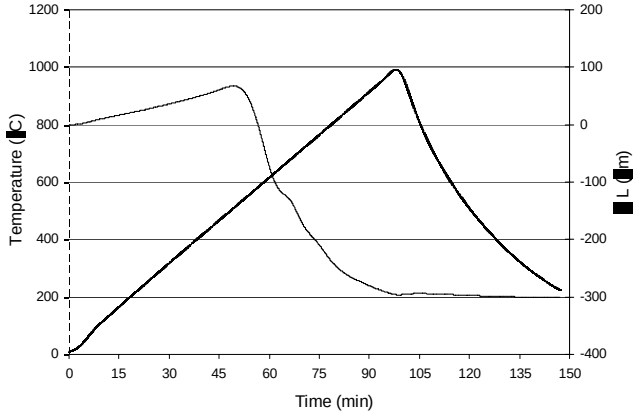

Figure 3. Carbonization cycle of BODA co-monomer **A**.

A dimensional loss of 9.7 % and 13.5 % was observed for co-monomer **A** in length and diameter, respectively. The thermal removal of volatile organic groups affords such dimensional dilation at 550 ºC. Upon further heating to 1000 ºC, the carbon yield was 81 %. Carbonization cycles at 1000 ºC for 24 hours produced no further dimensional change within the dilatometer's detectable limits. Monomer **1** and co-monomer **B** show similar geometry dilation compared to co-monomer **A**. Carbon yields were determined as 83 % and 81 % for monomer **1** and co-monomer **B**, respectively. These carbon yields are similar to BODA-derived carbonized structures reported elsewhere.[1]

The CTEs of the carbonized BODA samples were measured over a range of programmed temperatures as shown in **Figure 4**. Non-linear regions were observed for temperature ranges 20–300 ºC. This behavior is due the signal instability of the dilatometer over low temperature ranges. Linear CTE plots have been interpolated to include this range because the regression error analysis is minimal ($r^2 > 0.80$).

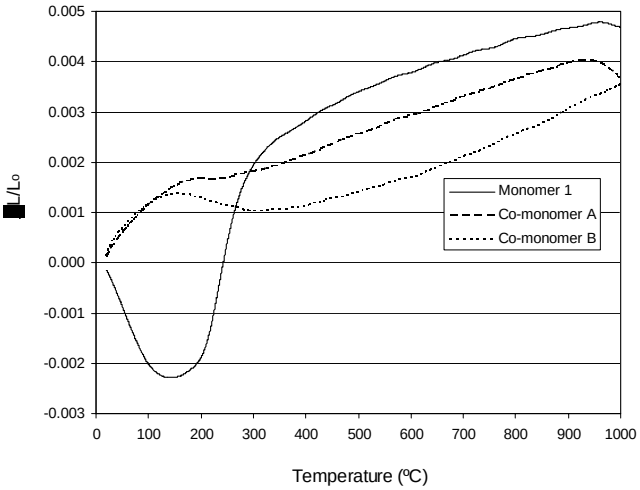

Figure 4. CTE profiles of monomer **1** and co-monomers **A** and **B** over temperature range.

Table 1 illustrates CTE analysis of glassy carbon samples derived from BODA monomer **1** and co-monomers **A** and **B**. Monomer **1** showed a notably higher T_{onset} compared with co-monomers **A** and **B**. The CTE values were observed for samples that were heat treated at 1500 ºC than for samples carbonized lower at 1000 ºC (compare entry 3 and 4). Carbonizing cured co-monomer **B** to 1500 ºC showed repeatable CTE values within 0.08 ($\times 10^{-6}$ C^{-1}) over the ranges 20-1000 ºC and 20-1500 ºC (compare entry 4 and 5).

Table 1. CTE Measurements Over A Range Of Heat Treatments For BODA Derived Glassy Carbon

Entry	Compound	T_{onset} (ºC)	HTT (ºC)	CTE α ($\times 10^{-6}$ C^{-1})	Std Dev ($\times 10^{-6}$ C^{-1})	Range (ºC)
1	**1**	575	1000	6.92	0.68	20-1000
2	**A**	545	1000	3.33	0.25	20-1000
3	**B**	540	1000	3.20	0.50	20-1000
4	**B**	535	1500	2.85	0.31	20-1000
5	**B**	535	1500	2.93	0.45	20-1500

Additional weight loss was observed for co-monomer **B** after being carbonized to 1500 ºC. This reduced the carbon yield to 65 % compared with 81% when carbonized to 1000 ºC. Upon STM analysis of co-monomer **B** heat treated at 1500 ºC showed evidence of graphitic regions possessing hexagonal distances of 2.46 Å on the Basal plane. Therefore, the observation of lower CTE values for co-monomer **B** heated to 1500 °C in comparison to samples heated to 1000 °C are a result of carbon reorientation to form planar graphite sheets inducing stronger π-π stacking interactions producing a more dense material. Furthermore, X-ray powder diffraction shows characteristic peaks of graphite, (002) and (110) planes, become narrower and taller at higher heat treatment temperatures (**Figure 5**).

Density measurements are also consistent with the observation of lowering CTE at higher HTTs. Densities of 1.608–1.651 g/cm^3 were observed for heat treated samples at 1000 ºC for monomer 1 and co-monomer **A** and **B**. The density was further lowered to 1.547 g/cm^3 and 1.405 g/cm^3 for co-monomer **B** at HTTs of 1500 ºC and 1700 ºC, respectively.

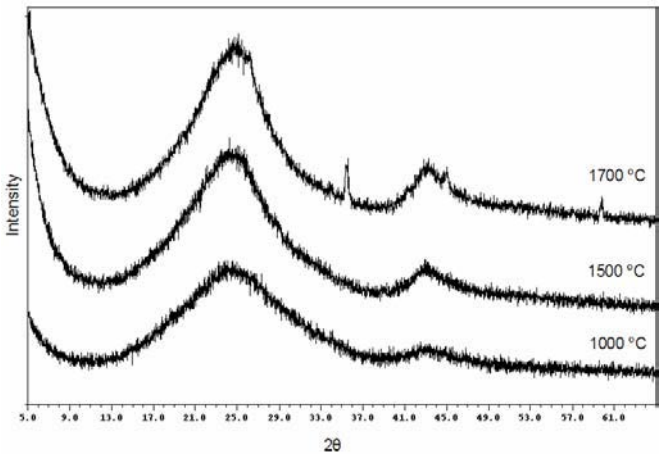

Figure 5. X-ray diffraction patterns for BODA-derived glassy carbon of co-monomer **B** as a function of heat treatment.

Conclusions

Dilatometry has provided insight to the thermal carbonization cycles of BODA polynaphthalenes. The onset of carbonization can be determined for each cured polymer providing a means to optimize thermal cycling. Furthermore, CTEs were determined for various BODA-derived glassy carbon systems to determine compatibility for MIMIC applications. We anticipate the use of these high carbon yield materials as potential use in fiber reinforced composites, mictrotubes, as well as other microdevices.

Acknowledgements. We gratefully acknowledge the Air Force Research Laboratory (AFRL) Space and Missile Propulsion Directorate for their financial support. We also thank Ms. Marietta Fernandez for microscopy and optical imaging support. S.T. Iacono's graduate studies are financially supported by the Air Force Institute of Technology Civilian Institution Program (AFIT/CIGD). D.W. Smith, Jr. is a Cottrell Scholar of the Research Corporation.

References

(1) Smith, D. W., Jr.; Babb, D. A.; Snelgrove, V. R.; Townsend, P. H.; Martin, S. J. *J. Am. Chem. Soc.* **1998**, *120*, 9078.
(2) Bergman, R.G. *Acc. Chem. Res.* **1973**, *6*, 25.
(3) John, J. A.; Tour, J. M. *J. Am. Chem. Soc.* **1994**, *116*, 5011.
(4) Kinoshita, K. *Carbon, Electrochemical and physiochemical properties*; Wiley-Interscience: New York, 1988.
(5) Perpall, M.; Perera, K. P. U.; DiMaio, J.; Ballato, J.; Foulger, S. H.; Smith, D. W., Jr. *Langmuir*, **2003**, 19, 7153.
(6) Zengin H.; Smith D. W., Jr. *Polymer Preprints* **2001**, *42(2)*, 427.
(7) Shah, H.V.; Brittain, S. T.; Huang, Q.; Hwu, S. J.; Whitesides, G. M.; Smith, D. W., Jr. *Chem. Mater.* **1999**, *11*, 2623.
(8) Shah, H. V.; Babb, D. A.; Smith, D. W., Jr. *Polymer* **2000**, *41*, 4415.
(9) Hoffman, W. P.; Phan, H. T.; Wapner, P. G. *Mat. Res. Innovat.* **1998**, *2*, 87.
(10) Perera, K. P. U.; Shah, H. V.; Foulger, S. H.; Smith, D. W., Jr. *Thermochimica Acta* **2002**, *388*, 371.

AFRL-PR-ED-TR-2006-0041
Primary Distribution of this Report:

AFRL/PRSM (3 CD + 2 HC)
Dr. Wesley P. Hoffman
9 Antares Road
Edwards AFB CA 93524-7401

AFRL/PR Technical Library (2 CD + 1 HC)
6 Draco Drive
Edwards AFB CA 93524-7130

Chemical Propulsion Information Agency (1 CD)
Attn: Tech Lib (Dottie Becker)
10630 Little Patuxent Parkway, Suite 202
Columbia MD 21044-3200

Defense Technical Information Center
(1 Electronic Submission via STINT)
Attn: DTIC-ACQS (Pat Mawby)
8725 John J. Kingman Road, Suite 94
Ft. Belvoir VA 22060-6218

AFRL/PROI (1 CD + 1 HC)
Mr. Ranney Adams
4 Draco Drive
Edwards AFB CA 7160